PHILOSOPHICAL TRANSACTIONS OF THE ROYAL SOCIETY A MATHEMATICAL, PHYSICAL & ENGINEERING SCIENCES

Radiation Hardening in Magnox Pressure-Vessel Steels

S. B. Fisher, J. E. Harbottle and N. Aldridge

Phil. Trans. R. Soc. Lond. A 1985 **315**, 301-332
doi: 10.1098/rsta.1985.0042

Phil. Trans. R. Soc. Lond. A **315**, 301–332 (1985) [301]
Printed in Great Britain

RADIATION HARDENING IN MAGNOX PRESSURE-VESSEL STEELS

By S. B. Fisher, J. E. Harbottle and N. Aldridge
Central Electricity Generating Board, Berkeley Nuclear Laboratories, Berkeley, Gloucestershire GL13 9PB, U.K.

(*Communicated by Sir Alan Cottrell, F.R.S. – Received 7 November* 1984)

[Plates 1–2]

CONTENTS

The ferritic steels used for reactor pressure vessels undergo a marked transition from ductile to brittle fracture behaviour over a relatively narrow temperature range. For most unirradiated mild steels the ductile to brittle transition temperature (d.b.t.t.) is between −50° and 20 °C. The process of irradiation hardening, through the formation of clusters of interstitial or vacancy defects, increases the friction stress of these steels and thereby raises the transition temperature.

Given the inherent tendency of these steels to fail in a brittle manner, the raising of the transition temperature under neutron irradiation poses a problem of considerable technological importance in the nuclear industry.

At the time (1962) when the first of the Central Electricity Generating Board (C.E.G.B.) Magnox nuclear stations began operation the phenomenon of brittle fracture was already comparatively well understood. A theory of the process had already been developed and applied to the problem of radiation embrittlement. However, as the results from the Magnox pressure–vessel surveillance scheme accumulated, it gradually became evident that the measured changes in yield stress in the monitoring specimens could not be accounted for simply on the basis of irradiation hardening through the formation of damage clusters.

By the late 1970s, sufficient data had been gathered from the surveillance programme to enable a detailed investigation of the processes occurring in the Magnox steels to be instituted. The form of the investigation was to subsequently evolve into two phases; an initial comprehensive microstructural study of the steels, followed by the formation of an interpretative model based on the observations.

In this paper we present the Magnox yield-stress monitoring measurements and then briefly describe the principal findings from our microstructural studies. The Magnox pressure-vessel steels contain between 0.05 and 0.4% by mass of copper and we show that under certain conditions this element may precipitate as small spherical particles within the matrix of the steels. A review of previous work on copper precipitation in ferrite is then followed by a description of our model. This assumes that the changes in yield stress generally arise from the combined effects of irradiation damage loops and copper precipitates. The formation of the latter may be enhanced by irradiation and in some steels their contribution is dominant. It is shown that the model successfully accounts for the measurements made on both plate and weld steels in all the Magnox stations.

Experimental support for the model comes from our own microstructural observations and from other studies, in the U.K. and elsewhere, using techniques which allow the detection of sub-microscopic particles in steels.

The model may be applied to pressure-vessel steels in other reactor systems. Indeed, it predicts that the yield-stress changes in steels with a high copper content irradiated under p.w.r. (pressurized water reactor) conditions will be dominated by the contribution from copper precipitation.

1. Introduction

The first two C.E.G.B. nuclear power stations, which were of the Magnox type, began operation in late 1962. Subsequently, in the period to 1966, four more stations of similar design were constructed. In all these stations the reactor pressure vessels were fabricated from low-carbon, mild steel plate.

The ferritic steels used for nuclear power reactor pressure-vessels undergo a marked transition from ductile to brittle fracture behaviour over a relatively narrow temperature range (*ca.* 80 K). For most unirradiated mild steels the ductile to brittle transition temperature (d.b.t.t.) is between −50° and 20 °C.

At the time when the Magnox reactors became operational, the phenomenon of brittle fracture was already comparatively well understood. A theory of the process had been developed and subsequently applied to the problem of radiation embrittlement (Cottrell 1961). The equation that Cottrell (1961) deduced from the brittle point is as follows,

$$(\sigma_i d^{\frac{1}{2}} + k_y) k_y = \beta G \gamma. \tag{1}$$

Here, d is the grain diameter in the steel, G is the shear modulus and γ is the effective surface energy of fracture. The parameter σ_i is the total friction stress due to obstacles that a dislocation meets as it crosses a glide plane. The parameter β (*ca.* 1 for tension) is an inverse measure of the hydrostatic component of the stress system and k_y is a measure of the difficulty of unpinning a dislocation to release it for glide. When the left side of this formula is smaller than the right side, the material is ductile; when larger, it is brittle.

This formula brings out the various mechanical and metallurgical factors that determine brittleness. In particular, Cottrell (1961) reasoned that the process of radiation hardening, through the formation of clusters of interstitial or vacancy defects, was very similar to precipitation hardening and would, by raising σ_i, raise the transition temperature in steels.

Cottrell (1961) adopted the following empirical relation to describe the radiation hardening in steels,

$$\Delta\sigma_y = A(\phi t)^{\frac{1}{3}}, \tag{2}$$

where σ_y is the yield stress, A is a constant, and $\phi t/(10^{18}\ \mathrm{cm}^{-2})$ is the slow neutron dose. He then used this equation to derive a semi-empirical expression for the resultant rise in transition temperature, ΔT/K.

$$\Delta T = 55(\phi t)^{\frac{1}{3}}. \tag{3}$$

Here, ϕt is the fast neutron dose. This formula, which was specifically designed to represent the most sensitive behaviour, suggested that over a 20 year life the transition temperature of a reactor vessel could rise by 50–100 °C.

Given the inherent tendency of ferritic steels to fail in a brittle manner, the raising of the transition temperature under neutron irradiation, by this amount, posed a problem of considerable technological importance in the nuclear industry. Cottrell (1961) suggested that for utmost security the vessel should have a built-in resistance to brittle fracture. He concluded that the only really safe course was to maintain the operating temperature above the fracture-propagation transition temperature.

While (3) gave a quantitative estimate of ΔT as a function of dose, the lack of knowledge at that time of the effects of irradiation variables (dose rate, spectrum, temperature) and material variables (heat treatment, compositions) on the degree of embrittlement made it desirable, if not essential, to *monitor* the changes in the properties of the steel in each reactor vessel over the lifetimes of the stations.

For this purpose, at the time of each Magnox reactor construction, Charpy V-notch and tensile specimens of the pressure-vessel steels, both plate and weld, were placed at various locations within, and close to, the main pressure envelope. These specimens are exposed to

temperature and flux conditions similar to the extremes found at the pressure vessel and batches of specimens are withdrawn periodically throughout the life of the vessel for testing. Comparison of the results of these tests with those from control tests on unirradiated material permits the estimation of the shift in transition temperature arising from neutron irradiation.

By 1965, sufficient data had been obtained from tests made on pressure-vessel steels irradiated in materials test reactors to enable a refinement of the relation between radiation hardening and neutron exposure to be made (Barton *et al.* 1965). It was found that a more accurate description of the process was given by the empirical relation,

$$\Delta\sigma_y = A(\phi t)^{\frac{1}{2}}, \tag{4}$$

where $\phi t/(10^{18}\ \mathrm{cm}^{-2})$ is the fission neutron dose, $\Delta\sigma_y$ is in units of 10^3 lbf in^{-2}† and A is a function of material composition and irradiation temperature. Barton *et al.* (1965) determined values of A between 2 and 17 for steels of relevant composition, over the temperature range $100° \leqslant T_{irr} \leqslant 360$ °C. They found that the hardening was strongly dependent on the aluminium or silicon contents of the steels. Little & Harries (1970) later attributed this dependence to the effect of 'free' nitrogen in the steels. They suggested that nitrogen, in solution, was able to stabilize the damage cluster or loops or to refine their density. They postulated that the role of aluminium or silicon was to reduce the level of free nitrogen in the steels through the formation of stable nitrides when the steels were heat treated.

The relation (4) formed the bench-mark against which the results of the yield-stress monitoring scheme tests were assessed.

The initial monitoring withdrawals from the lead Magnox stations were made at annual intervals. The results from these early withdrawals confirmed that the change in properties lay within the expected range. Subsequently, the periods between withdrawals were extended. It was not until the mid-1970s, when the results from withdrawals made from all the stations were available, that it became clear that the changes in properties, although acceptably small, were not conforming to (4).

By this time, work in the United States on steels for the pressure vessels, which were irradiated at *ca.* 290 °C, had proved the role of copper in increasing their sensitivity to radiation hardening (Potapovs & Hawthorne 1969). However, no mechanism for the influence of this particular element was established. While the composition and heat treatment of the p.w.r. pressure-vessel steels are broadly similar to those for the Magnox steels, it was far from obvious at that time that copper was playing a similar role in our monitoring specimens. In the event, it was decided to institute a detailed investigation of the mechanism(s) of radiation hardening in the Magnox pressure vessel steels.

A comprehensive microstructural study of selected surveillance specimens both in the irradiated and unirradiated conditions, was followed by the formulation of a model for radiation hardening based largely on the observations. The results of the microstructural studies were reported in some detail, together with a brief description of the basis of our model, at the British Nuclear Energy Society Conference in Brighton in April, 1983 (Fisher *et al.* 1984*a*). In this paper we present the following.

(i) The Magnox monitoring results from tensile specimens.

(ii) A brief description of our microstructural studies.

† 1 lbf in $^{-2} \approx 6895$ Pa.

PHILOSOPHICAL TRANSACTIONS OF THE ROYAL SOCIETY A MATHEMATICAL, PHYSICAL & ENGINEERING SCIENCES

(iii) A review of previous work on the behaviour of copper in thermally aged, but unirradiated iron–copper alloys and ferritic steels containing copper.

(iv) The formulation of our model for radiation hardening and a comparison of its predictions with the results from the monitoring scheme.

2. The monitoring scheme

Our principal objective in this paper is to present an interpretation of the yield-stress monitoring results from the plate and weld steels irradiated in the five Magnox stations from which sufficient data are available. We shall refer to these stations throughout this report as stations 1–5. The results from the monitoring scheme may be broadly classified into two categories: those pertaining to 'low'-temperature (170–225 °C) locations in the reactor and those from 'high'-temperature locations (290–400 °C). Here, we shall mainly concern ourselves with the former category, because, in general, the results from the 'hot' locations are much less significant. However, there are important exceptions to this statement and we shall also examine these in considerable detail.

The appropriate plate and weld specimens for each station were usually exposed in both 'cold' and 'hot' locations and in three of the five stations specimens were located in two low-temperature positions with significantly different conditions of exposure. With the exception of station 1, the weld steel specimens were taken from submerged-arc machine welds because this process was employed extensively in the construction of the vessels in the other stations. The pressure vessels in the two reactors of station 1 were fabricated completely by manual welding and the corresponding surveillance specimens are representative of this method of fabrication. The station 5 monitoring scheme contained no submerged-arc machine weld specimens although this material was used in reactor construction.

Table 1. Compositions of plate steels in cold locations

percentage by mass

station	C	Si	Mn	S	P	Cu	Ni	Mo	Al
1	0.19	0.3	1.22	0.027	0.015	0.12	0.11	0.03	0.01[a]
2	0.09	0.37	1.05	0.02	0.015	0.06	0.06	[b]	0.008
3	0.11	0.13	1.1	0.02	0.015	0.4	0.07	0.23	0.018
4	0.15	0.16	1.3	0.035	0.02	0.09	0.06	0.01	0.05
5	0.17	0.25	1.1	0.034	0.016	0.15	0.08	0.02[a]	0.02[a]

[a] Indicates upper limit.
[b] Indicates value not determined.

2.1. *The steel compositions*

The chemical compositions of the plate steels irradiated in the low-temperature locations of the five Magnox stations are listed in table 1. In general, the same plate steels were also exposed in the corresponding hot locations in each station. Here, we shall only examine the results from the plate steels in those positions where the temperature of exposure was greater than *ca.* 340 °C. Only the station 1 and station 3 results fall into this category. In addition to the two steels listed in table 1 for these stations a further steel was exposed in the hot locations in station 3. For convenience, the compositions of all three steels, relevant to our examination of high-temperature behaviour, are included in table 2.

Table 2. Compositions of plate steels in hot locations

percentage by mass

material	C	Si	Mn	S	P	Cu	Ni	Mo	Al
station 1 plate	0.19	0.3	1.22	0.027	0.015	0.12	0.11	0.03	0.01[a]
station 3 plate (steel I)	0.11	0.13	1.1	0.02	0.015	0.4	0.07	0.23	0.018
station 3 plate (steel II)	0.14	0.1	1.1	0.03	0.013	0.12	0.015	0.01	[b]

[a] Indicates upper limit.
[b] Indicates value not determined.

Table 3. Compositions of the weld steels

percentage by mass

station	C	Si	Mn	S	P	Cu	Ni	Mo	Al
2	0.06	0.65	1.3	0.03	0.03	0.25	0.08	0.02	0.004
3	0.09	0.72	1.2	0.03	0.03	0.2	0.08	0.01	0.008
4	0.06	0.46	1.6	[a]	[a]	0.16	0.1	0.02	0.012

[a] Indicates values not determined.

Note that, for ease of reference, the two steels exposed in station 3 are referred to as steels I and II, steel I having the high copper content (*ca.* 0.4 % by mass).

The compositions of the submerged-arc machine weld steels exposed in the low-temperature locations of the monitoring scheme in stations 2, 3 and 4 are given in table 3.

Unfortunately no analysis was performed for the manual weld specimens exposed in station 1. As we shall see, this did not constitute a handicap in the interpretation of the results for this material.

In addition to the plate and machine weld specimens listed above, the Magnox monitoring scheme contains specimens relevant to other materials of construction. These include samples of forgings and manual weld. At the present time the yield-stress monitoring results from these other materials are only available for station 4.

Here, apart from the plate and machine weld specimens whose compositions have already been listed in tables 1 and 3, specimens of manual weld and two types of forging are also irradiated. The compositions of these materials are listed in table 4, together with those for the plate and machine weld. The yield-stress results from these materials, when taken together, were to prove of considerable value in the formulation of an overall interpretation of the whole of the monitoring scheme results. For this reason particular care was taken in establishing the composition of these steels, especially the copper content. In addition to wet chemical analyses of control specimens, electron microprobe analyses for copper content were performed on both unirradiated and irradiated samples. In one case, forging 1, significantly different copper contents were measured in irradiated samples withdrawn and tested in consecutive years, after 13 and 14 years of operation (see table 4).

2.2. *The exposure conditions*

The temperatures and neutron fluxes pertaining to the low-temperature locations in the five stations are listed in table 5.

Flux measurement at most of the locations of interest was principally by the detection of the

Table 4. Compositions of the station 4 steels

percentage by mass

material		C	Si	Mn	S	P	Cu	Ni	Mo	Al
plate	a[1]	0.15	0.16	1.3	0.035	0.02	0.09	0.06	0.01	0.05
	c[1]	—	—	—	—	—	0.09	—	—	—
machine weld	a	0.06	0.46	1.6	[2]	[2]	0.16	0.1	0.02	0.012
	b[1]	—	—	1.5	—	—	0.17	—	0.01	0.03
	c	—	—	—	—	—	0.16	—	—	—
manual weld	a	0.08	0.45	0.9	0.027	0.025	0.06	0.06	[2]	[2]
	c	—	—	—	—	—	0.06	—	—	—
forging 1	b	0.09	0.25	1.6	—	—	0.09	—	—	—
	c	—	—	—	—	—	0.11[3]	—	—	—
	c	—	—	—	—	—	0.08[3]	—	—	
forging 2	a	0.18	0.36	1.3	0.024	0.024	0.1	0.08	0.01	0.049
	c	—	—	—	—	—	0.07	—	—	—

[1] a = wet chemical analysis; b = microprobe analysis; c = microprobe analysis of irradiated tensile samples; a, b from R. B. Jones (personal communication); c from S. B. Fisher (unpublished work).

[2] Indicates not determined in wet chemical analysis.

[3] Microprobe analysis for forging 1 samples withdrawn after 13 and 14 years were significantly different.

Table 5. Exposure conditions for cold locations

station (location)	irradiation temperature/°C	fission flux / $cm^{-2}\ s^{-1}$	operating factor (percentage)	spectrum type
1	167	10^7	80	below-core
2 (1)	190	8.1×10^8	82	below-core
2 (2)	190	1.6×10^9	82	side-core
3 (1)	170	4.4×10^7	87	below-core
3 (2)	170	1.7×10^7	87	below-core
4	225	3.8×10^8	87	below-core
5 (1)	221	5.8×10^8	85	side-core
5 (2)	190	1.5×10^8	85	below-core

$Fe^{54} \rightarrow Mn^{54}$ reaction. In each case the flux was determined as an equivalent fission flux, ϕ_f. The value of ϕ_f calculated for different reactions may vary by a factor of two because the actual fast flux at a detector does not have a fission spectrum. Therefore, while the absolute value of ϕ_f determined from one reaction is uncertain, the use of one principal reaction at all locations with similar spectra minimizes the relative error in flux levels between different positions.

In one location, referred to as 3(2), the flux measurements are suspect and it is possible that the actual flux at this position is a factor of two times the value given in table 5.

Complete spectral information corresponding to all the relevant monitoring positions is not yet available. However, all the locations of interest may be classified as either 'below-core' or 'side-core' (table 5). There is sufficient knowledge of the spectra in these general areas in Magnox stations to permit the approximate calculation of atomic displacement rate from the equivalent fission flux, ϕ_f. The total atomic displacement rate, K, at any location may be expressed in terms of a displacement rate, K_f, calculated from the fission flux,

$$K_f = \sigma_d^f \phi_f; \quad K = \epsilon K_f, \tag{5}$$

where σ_d^f is the average displacement cross section for a fission (Watt) spectrum. For the side-core and below-core locations, respectively, $\epsilon_s \approx 3$ and $\epsilon_b \approx 13$.

The yield-stress data given in §2.3 are plotted as a function of years of operation. The fission doses corresponding to these years of operation refer to actual periods of irradiation, which may be significantly less. Detailed examination of the operating histories of the five stations allowed the real time of irradiation, t, to be expressed as a function of the years of operation via an 'operating factor', such that

$$t\ (\text{years}) = \text{years of operation} \times \text{operating factor}. \tag{6}$$

The operating factors for the five stations are also shown in table 5. It should be stressed that the fluxes, ϕ_f, shown in the tables are the actual fluxes at the locations when the reactor is at power.

2.3. *The monitoring results*

Figure 1 shows the results from yield-stress measurements made on all the plate monitoring specimens irradiated in the cold locations in the five Magnox stations. The results are plotted as the change in yield stress (positive for an increase in strength) against years of operation. Considering the differences in irradiation temperature, flux and material composition between locations the wide variation in the results is not surprising. However, these results defy any general interpretation on the basis of the simple empirical relation (4) determined by Barton *et al.* (1965) and this relation includes these fundamental parameters. This failure will be illustrated when we come to compare the results of our model with the monitoring data.

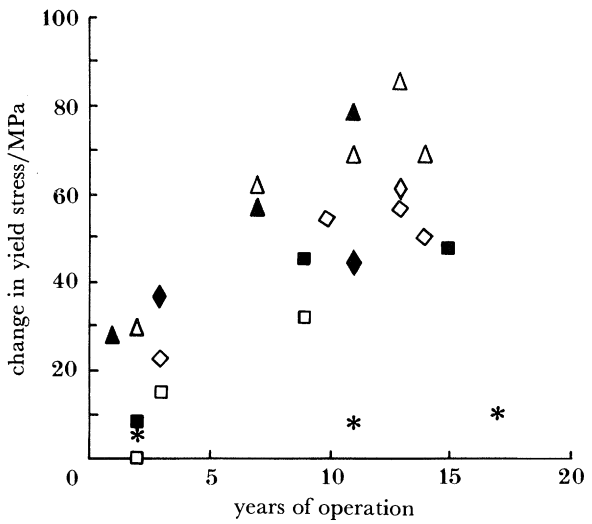

FIGURE 1. Change in yield stress as a function of years of operation for plate steels exposed in low-temperature locations. *, Station 1; ▲, station 2(1); △, station 2(2); ■, station 3(1); □, station 3(2); ◇, station 4; ◆, station 5(1); ◊, station 5(2).

In addition to the above comments, there is no obvious correlation between the results and the copper content of the specimens. Indeed the steel containing the highest copper content (*ca.* 0.4% by mass) in station 3, shows a comparatively small increase in strength, while the steel containing the least copper (*ca.* 0.05% by mass) in station 2, shows the largest increases in yield stress. The monitoring samples (*ca.* 0.12% by mass of copper) in station 1 show virtually no effect of irradiation. Looked at in isolation, the cold exposure results for plate steels are a

clear indication of the inadequacy, in the context of Magnox irradiations, of the Barton *et al.* (1965) relation, but yield no suggestion for a possible interpretation. Figure 2 shows the yield-stress results from the station 1 and station 3 plate steels exposed in hot locations (340–390 °C). Clearly the high copper (0.4% by mass) steel, steel I, in station 3 is significantly more sensitive than the lower copper (0.12% by mass) steel, steel II, which was irradiated under identical conditions. The station 1 steel plate, also containing *ca.* 0.12% by mass of copper, behaves in similar fashion to steel II.

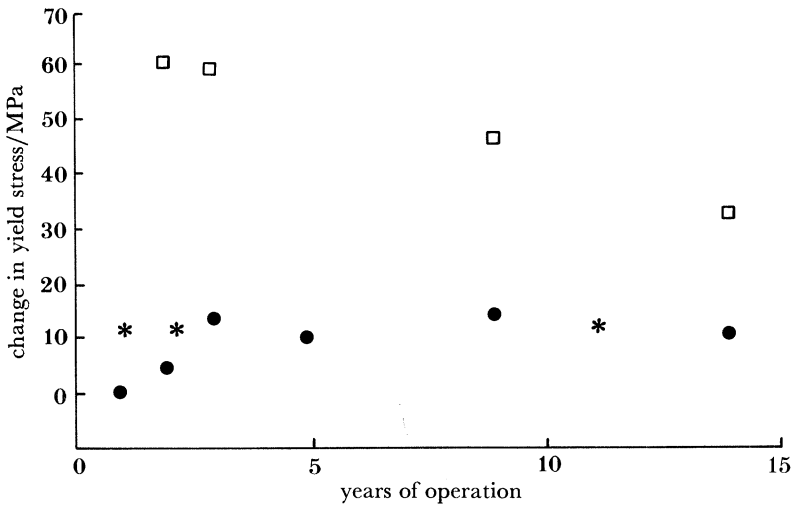

FIGURE 2. Change in yield stress as a function of years of operation for plate steels I & II exposed at 390 °C in station 3 and the station 1 steel exposed at 340 °C. □, Station 3 (steel I); ∗, station 1; ●, station 3 (steel II).

The comparatively large increase in strength in the 0.4% by mass of copper plate is present after only two years of operation and subsequently decreases with exposure. This, in itself, is indicative of an overageing phenomenon and this conclusion is supported by the knowledge that at this irradiation temperature (390 °C) the contribution of irradiation damage to $\Delta\sigma_y$ is negligible (Barton *et al.* 1965). These high-temperature results are therefore the first indication that the 'precipitation' of copper is playing a significant role in the behaviour of these steels. Figure 3 shows the yield-stress data from all the monitoring specimens, plate, forgings and weld, exposed in station 4. Here they are again plotted against years of operation. These results, with the same conditions of irradiation temperature (225 °C) and dose for each material, do seem to indicate an increasing sensitivity to irradiation with increasing copper content. Note in particular the difference between the results of forging 1 obtained on nominally the same material after, respectively, 13 and 14 years of operation. The higher yield-stress change after 13 years may well be a result of the high copper content of the particular specimen tested at that time. In this context, only the manual weld results appear anomalous, particularly when compared with the data from forging 2, which has the same copper content. As we shall see in the following sections, this observation is of considerable significance. Figure 4 shows the yield-stress data from the weld steels irradiated at low temperatures in stations 1–4. The manual weld results from station 1 are similar to those from the corresponding plate, there being no significant increase in strength in either material. In station 3 the weld (*ca.* 0.2% by mass of copper) is less sensitive than the high copper plate (0.4% by mass), while in stations 2 and

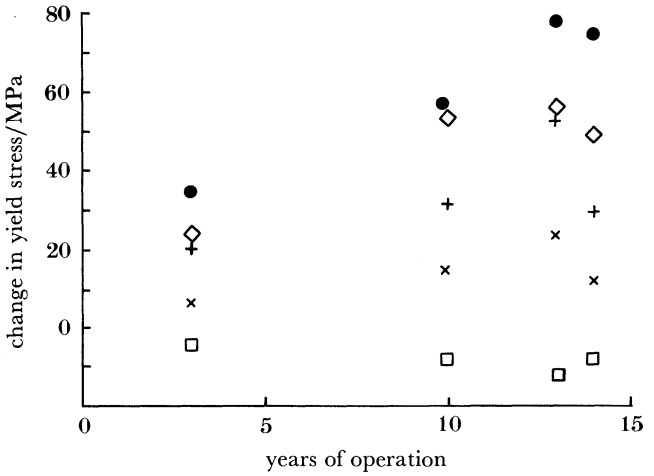

FIGURE 3. Change in yield stress as a function of years of operation for the steels exposed in station 4. ●, Machine weld; □, manual weld; ◇, plate; + forging 1; × forging 2.

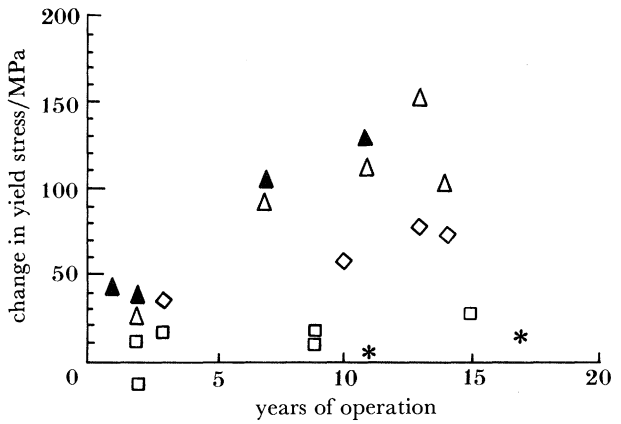

FIGURE 4. Change in yield stress as a function of years of operation for the weld steels exposed in low-temperature locations in stations 1–4. ✱, Station 1; △, station 2(2); ▲, station 2(1); □, station 3; ◇, station 4.

4 the welds (*ca.* 0.2% by mass of copper) are considerably more sensitive than their corresponding plate steels. Taken together with the results on all materials in station 4, the weld data are a clear indication of the influence of copper.

3. MICROSTRUCTURAL STUDIES

Our microstructural studies may be divided into three categories.

(i) A comparison of the structures of control specimens and low-temperature exposed samples irradiated in station 4. Plate, manual and machine welds were all examined.

(ii) The examination and comparison of unirradiated control specimens of plate and weld, before and after stress relief.

(iii) The examination of unirradiated, but long-term aged, specimens of the monitoring steels for station 3.

Throughout the work, emphasis was placed on the characterization of matrix precipitates or particles, the measurement of volume fraction and the measurement of dislocation density. Thin foils and carbon extraction replicas were prepared from all the materials studied.

The examinations were performed on either a Philips EM400 with a Kevex analytical facility, or on a Hitachi h.v.m. (high-voltage microscope) operating at 400 keV. Precipitate identifications were by combined energy dispersive–electron diffraction techniques. Diffraction pattern measurements were made on an HP 9874A digitizer interfaced to HP 9825 and HP 9836 computers. Analysis of the patterns was automatic, using software written by the authors.

The examinations in categories (i) and (ii) above have been described in detail in internal laboratory reports (see, for example, Fisher *et al.* (1982) and elsewhere (Fisher *et al.* 1984*a*; Harbottle & Fisher 1982). Here, we shall only summarize the principal findings of this work and give one or two specific examples to illustrate the techniques employed. The studies in category (iii) above have only previously been described in an internal laboratory report (Fisher *et al.* 1984*b*); we shall examine these in some detail here.

3.1. *Comparison of unirradiated and irradiated specimens*

The specimens examined in this category were the plate, manual and machine welds pertaining to the station 4 monitoring scheme. The irradiated samples had received a dose *ca.* 2×10^{17} neutrons cm^{-2}, at an irradiation temperature *ca.* 225 °C in Station (4). The initial heat treatment of the plate steels, before irradiation, was the standard normalization at 900 °C for 6 h with subsequent stress relief at 600 °C h along with the welds. The 'macrostructures' of the plate and weld resulting from this heat treatment are illustrated in figure 5, plate 1. The plate is ferrite–pearlite with a relatively uniform grain size. The welds, in contrast, exhibit two distinct grain types, fine (recrystallized) and columnar, running in bands along the weld. All the welds contained regions of bainite.

The micrographs in figure 5 were taken from carbon extraction replicas. Even at this low level of magnification the high density of matrix precipitates in both plate and weld can be clearly seen.

Initial examinations of thin foil samples of the plate and weld in both unirradiated and irradiated conditions were performed in the h.v.m. These confirmed the presence of the matrix precipitate and allowed the measurement of the dislocation density in all materials. In all the plate samples the density was found to be *ca.* 3×10^9 cm^{-2}. In the welds the density varied from *ca.* 10^{10} cm^{-2} in the fine-grain regions to *ca.* 3×10^{10} in the columnar grains. No measurable differences were detected between controls and irradiated specimens.

Precipitate identification was performed on the EM400. Thin foils and carbon replicas were examined. Again, no differences in either character or density of the precipitates were found between irradiated and unirradiated samples. The results may be summarized as follows.

(i) In all, thirteen precipitate phases were identified in the mild steel weld or plate. Most of these were only present in the welds and included sulphides of copper, iron and zinc; oxides of iron; the double oxides, cadmium iron oxide and manganese titanate; nitrides of silicon, manganese and aluminium; carbides of titanium and vanadium.

(ii) The principal precipitates identified in the welds were copper sulphide and the silicon–manganese nitride, (Si, Mn) N. Figure 6 shows examples of their identification by combined X-ray analytical–diffraction techniques. While the volume fraction of (Si, Mn) N was found to be approximately the same, *ca.* 0.3%, in all the welds, the volume fraction of

copper sulphide varied from less than *ca.* 0.03% in the machine welds (which contained *ca.* 0.16% by mass copper) to *ca.* 0.08% in the manual weld (which contained only 0.06% by mass copper). Some 0.04% by mass of the copper in the manual weld was therefore present as a fine (*ca.* 20 nm diameter) dispersion of copper sulphide particles. This finding is of significance in relation to the monitoring results from station 4 as we shall see in subsequent sections. The particular phase of copper sulphide identified was $Cu_{18}S$ (digenite I). This was the first observation made of copper sulphide as a matrix precipitate in mild steels (Harbottle & Fisher 1982).

(iii) In the plate steels, aluminium nitride was the sole phase detected. This compound is virtually isomorphous with the (Si, Mn) N found in the weld materials and the two phases can only be distinguished with certainty with the use of energy dispersive X-ray analysis. The precipitates ranged in diameter from 40 to 100 nm, with a volume fraction *ca.* 0.3%.

3.2. *The influence of stress relief*

The work on the station 4 monitoring steels established the presence of copper sulphide in the weld materials and also confirmed the existence of stable nitrides in both plate and weld steels. In the latter, it substantiated the hypothesis of Little & Harries (1970) that the 'free' nitrogen in these materials is controlled by the presence of aluminium, silicon and manganese.

The work was subsequently extended to investigate the influence of stress relief on the formation of these nitrides. Samples of actual pressure-vessel 'cut-outs' were obtained. These had been cut from the vessel before stress relief. The examination of these specimens established the following points.

(i) Aluminium nitride (AlN) is formed in plate material if the material is slow cooled after a prolonged anneal at *ca.* 900 °C. The formation of this phase must deplete the steel of soluble nitrogen.

(ii) During subsequent welding of the plates the AlN in the heat affected and molten zones returns to solution above *ca.* 1200 °C and is prevented from reforming as a result of the rapid cooling that ensues.

(iii) During the stress relief at 600 °C, the nitrogen, now in solution in the welded region, is free to form the silicon–manganese nitride, (Si, Mn) N.

The efficiency of nitrogen removal in welds is therefore dependent on the levels of silicon and manganese present and on the duration of the stress relief. The fact that no (Si, Mn) N is formed in this plate steel on stress relief is an indication of the effectiveness of the AlN formation in removing soluble nitrogen.

The copper sulphide precipitate in the welds was found to be present both before and after stress relief in the same form. This confirmed that this phase is probably formed following a high temperature oxidation reaction during welding (Harbottle & Fisher 1982).

As well as confirming the influence of aluminium and silicon on the levels of soluble nitrogen in pressure-vessel steels, this work provided an explanation for the variability in yield stress between the control steels in the Magnox monitoring scheme (Fisher *et al.* 1984*a*).

3.3. *Long-term ageing of steels*

The two plate steels examined in this work were controls from the monitoring scheme for station 3. Their compositions were given in table 2, where they are referred to as steels I and II with copper contents respectively of *ca.* 0.4% and 0.12% by mass. The yield-stress

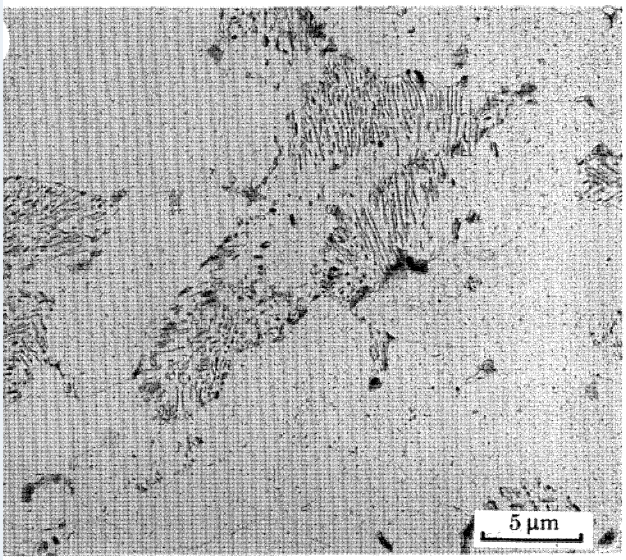

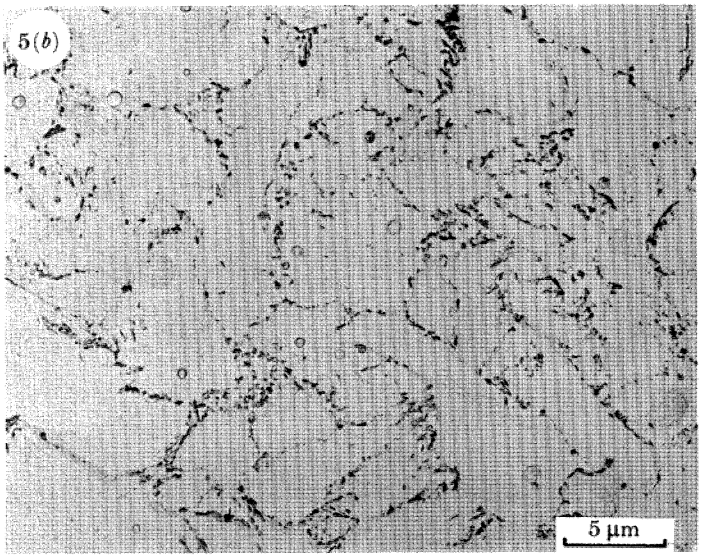

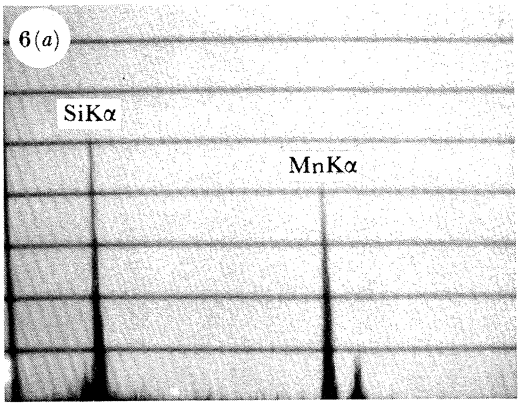

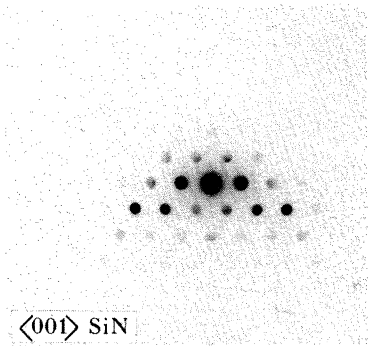

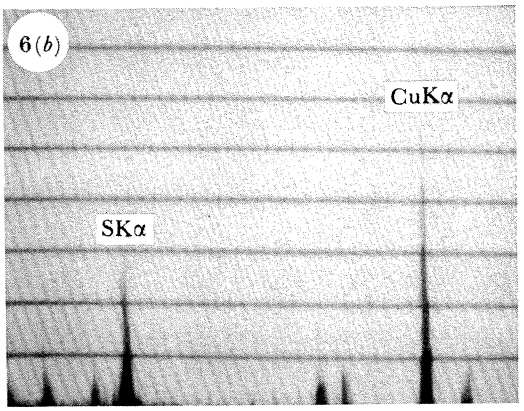

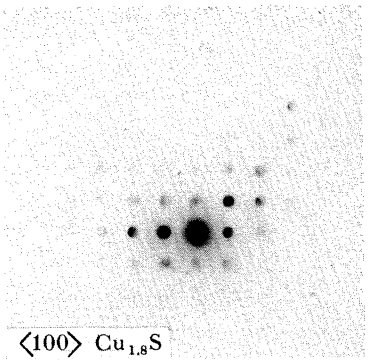

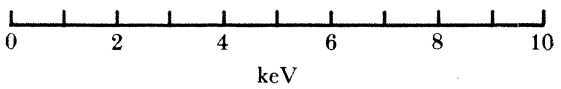

FIGURE 5. The general macrostructures of (*a*) plate and (*b*) weld steels as revealed by carbon extraction replicas.

FIGURE 6. The identification of (*a*) (silicon, manganese) nitride and (*b*) copper sulphide precipitates by using a combination of electron diffraction and X-ray energy analysis techniques.

(*Facing p.* 312)

PHILOSOPHICAL TRANSACTIONS OF THE ROYAL SOCIETY A MATHEMATICAL, PHYSICAL & ENGINEERING SCIENCES

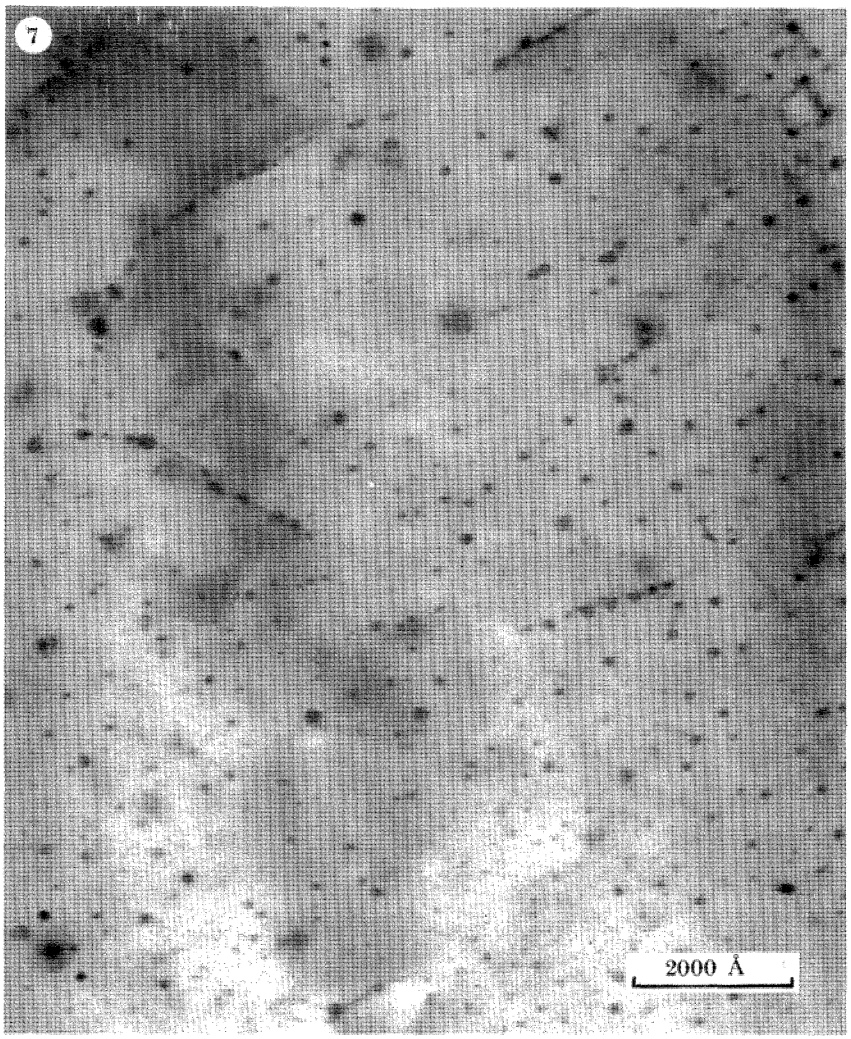

FIGURE 7. Spherical copper precipitates identified in a thin foil of steel I examined in an EM400. The particles are present on both dislocations and within the matrix of this steel after ageing at *ca.* 350 °C for 19600 h. The average precipitate diameter is *ca.* 140 Å, and the volume fraction precipitated is *ca.* 0.35 %.

PHILOSOPHICAL TRANSACTIONS OF THE ROYAL SOCIETY A MATHEMATICAL, PHYSICAL & ENGINEERING SCIENCES

monitoring data from these steels exposed in the 'hot' locations in station 3 were given in figure 2. The temperature of exposure was *ca.* 390 °C, and after only two years of operation, corresponding to a fission dose of only *ca.* 2×10^{16} cm^{-2}, steel I showed an increase in yield stress of *ca.* 60 MPa. Under these irradiation conditions no significant increase in strength is expected to arise from irradiation damage (Barton *et al.* 1965).

The two control steels were aged at a temperature (*ca.* 350 °C) similar to that in their 'hot' locations, for 19600 h (*ca.* $2\frac{1}{4}$ years). Tensile test specimens were cut from the steel I samples to determine the change in yield stress on ageing. Microscopy was performed on the controls before and after ageing and also on the tested tensile specimens of steel I. The results are described in detail in an internal laboratory report (Fisher *et al.* 1984*b*), but may be summarized in the following manner.

(i) In the 0.4% by mass of copper steel (steel I), copper precipitated on dislocations and throughout the ferrite matrix as a result of the ageing treatment (figure 7, plate 2). Virtually the whole of the copper in this steel was precipitated as fine, *ca.* 14 nm diameter, spherical particles of f.c.c. copper.

(ii) In steel II, containing only *ca.* 0.12% by mass of copper, less than half the available copper precipitated as particles *ca.* 10 nm diameter. The nucleation in this instance was confined to dislocations.

(iii) In the high-copper steel, which also contained *ca.* 0.25% by mass of molybdenum, molybdenum carbide particles were also precipitated on ageing at 350 °C. However the nucleation of this phase was restricted to pre-existing AlN precipitates.

(iv) The yield stress of steel I was increased by *ca.* 68 MPa as a result of the ageing. Russell & Brown (1972) derived equations for the increase in strength in ferrite containing a dispersion of copper precipitates. The measured increase in strength in steel I, for the measured volume fraction and size of precipitate, is entirely consistent with their theory.

The results of these studies, when compared with the monitoring measurements made on the same steels exposed under similar conditions, are a clear indication that copper precipitation is playing a significant role in the behaviour of the Magnox monitoring steels exposed in hot locations. In §4.4 these ageing results will be discussed further in conjunction with the Russell & Brown (1982) theory. This discussion forms a significant part of a general examination of the precipitation of copper in ferritic steels.

4. Copper precipitation in ferrite

Our microstructural studies of the Magnox steels irradiated at 225 °C in station 4 revealed no direct evidence to support the idea that copper influenced the radiation sensitivity of these materials. However, the results from the long-term aged steels clearly established the overwhelming importance of copper precipitation in steels exposed at high temperatures. These studies were performed over the period 1979–1982 and during this time further support for this mechanism of copper-enhanced radiation sensitivity came from overseas. The small-angle neutron scattering (s.a.n.s.) and field-ion microscopy–atom probe (f.i.m.–a.p.) studies of Frisius & Bünemann (1979) and Lott *et al.* (1981) respectively, showed that the aggregates responsible for hardening in irradiated iron–copper alloys and p.w.r.-type pressure-vessel steels were rich in copper, small (2–6 nm), but present in high density (10^{17}–10^{18} cm^{-3}). These results appeared quite similar to those that had been obtained earlier by f.i.m.–a.p. (Goodman *et al.* 1973) in

iron–copper alloys thermally aged to maximum strength. Not only did these experiments point to the mechanism of the role of copper, but the findings also suggested, in the small size of the 'precipitates' observed, a reason why we were unable to detect their presence in our steels from station 4. With a diameter of only 2–6 nm these particles would have been well below the practical resolution limit of electron microscopy in these steels.

A consideration of all these factors led us to undertake a detailed review of previous studies of copper precipitation in ferrite.

4.1. *Previous ageing studies*

The solubility of copper in α-iron between 700–850 °C has been determined by Wriedt & Darken (1960). They found that the line best representing the limit of the α-field is given by

$$\lg(\text{percentage by mass of copper}) = 4.335 - 4499\,T^{-1}, \tag{7}$$

where T is measured in kelvins. Extrapolation of this relation beyond the temperature region examined suggests that the solubility is effectively zero (less than 0.01 %) below 430 °C.

There have been a number of careful studies of the strengthening accompanying the precipitation of copper on ageing iron–copper alloys (Hornbogen & Jung 1964; Fujii *et al.* 1968) and ferritic steels (Krishnadev & Le May 1970). The most comprehensive results are those of Fujii *et al.* (1968). These are reproduced in figure 8. These workers examined the strengthening in a wide range of alloys, containing an atomic percentage of 0.6–6 % copper, on ageing at temperatures between 400–700 °C. It is clear from the figure that even small concentrations of copper are capable of producing large increases in yield stress on ageing. An atomic copper content of *ca.* 0.6 % increases the yield stress by *ca.* 200 MPa at peak strength. The results indicate that for a given ageing temperature, T_a, the time to peak strength, t_p, is virtually independent of copper content provided T_a is sufficiently below the solubility temperature for the lowest copper content considered. For example, at $T_a = 600$ °C, alloys with atomic percentages of copper between 1.8–6.0 % have the same t_p of *ca.* 0.2 h. At $T_a = 500$ °C, $t_p \approx 1$ h for alloys with atomic percentages of copper between 1.4–6.0 %. Clearly as T_a decreases the lower bound on copper content for an alloy to display the same t_p as those with high contents also decreases. The results also show that for a given copper content the maximum strengthening is virtually independent of ageing temperature, again, provided that T_a is sufficiently below the appropriate solubility temperature.

Krishnadev & Le May (1970) measured the variation in hardness of a ferritic steel containing 2 % copper as a function of ageing time at temperatures between 425–700 °C. Their observations, in terms of the measured times to peak strength, are entirely consistent with the measurements of Fujii *et al.* (1968).

If we assume a relation of the type (Burke 1965)

$$\ln t_p = \text{constant} + E/kT_a \tag{8}$$

for the precipitation reaction, where E is an effective activation energy for the process and T_a is measured in kelvins, we can incorporate the results of both groups of workers and represent them graphically as in figure 9. Here the results are enclosed within the pair of parallel lines in the figure. The lines are extrapolated to lower temperatures. Figure 9 constitutes a summary of the kinetics of copper precipitation. Included in the figure are 'C' curves for iron–copper

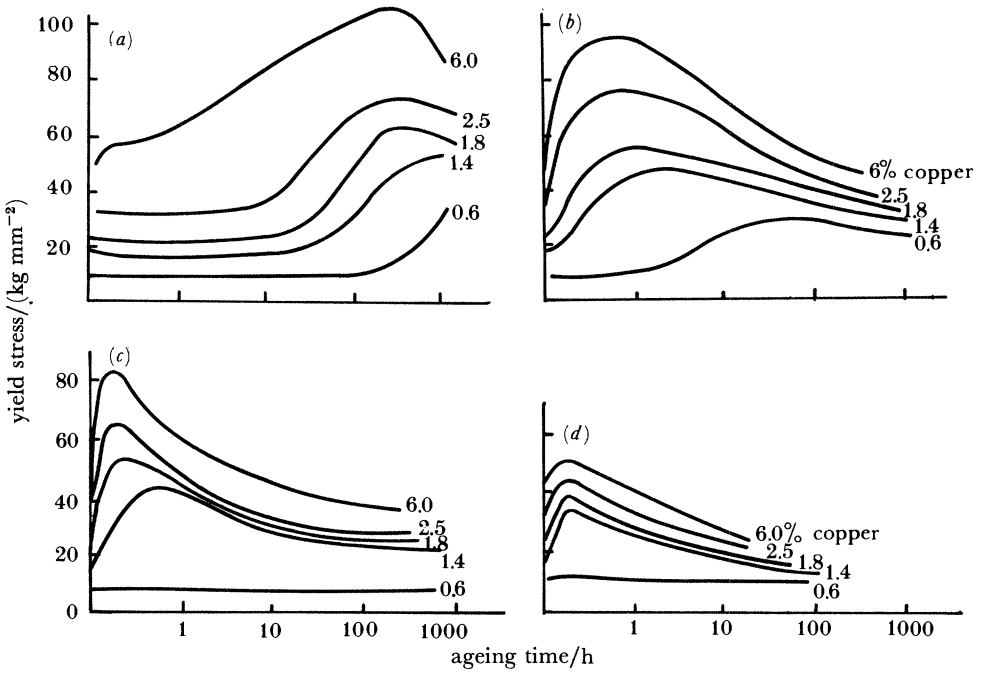

FIGURE 8. Room-temperature yield-stress measurements on iron–copper alloys as a function of ageing time at ageing temperatures of (*a*) 400, (*b*) 500, (*c*) 600, (*d*) 700 °C (after Fujii *et al.* 1968).

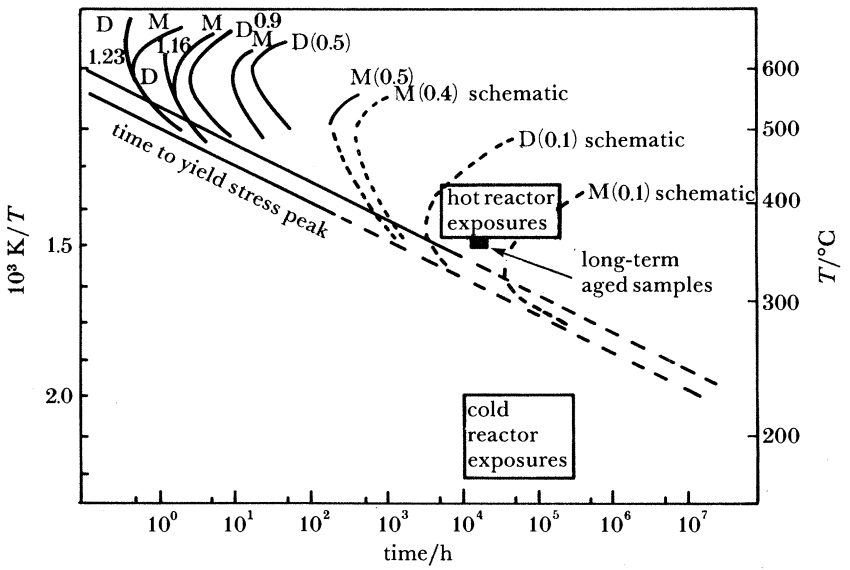

FIGURE 9. A comparison of Magnox exposure conditions with data from iron–copper alloys. The 'C' curves are from Hornbogen & Jung (1964) and the plot of time to peak strength as a function of inverse temperature from Fujii *et al.* (1968). The copper content for each 'C' curve is shown. The symbols D, M refer to dislocation or matrix nucleation.

alloys, extracted from the work of Hornbogen & Jung (1964). They examined alloys with copper contents ranging from 0.5–1.23 % by mass at ageing temperatures between 500–750 °C. They showed that, for these particular alloys aged within this range of temperatures, precipitation may take place initially on dislocations, with subsequent nucleation within the matrix. Two maxima, corresponding to these separate events, were generally detected in measurements of yield stress with ageing. The 'C' curves corresponding to these maxima are labelled D and M, for dislocation and matrix nucleation, in figure 9.

The results of Hornbogen & Jung (1964) are compared with the plot of lg t_p against ageing temperature in figure 9. It is clear from this comparison why Fujii *et al.* (1968) found only a single peak in their yield-stress measurements. For atomic copper contents above 1.4 %, dislocation and matrix precipitation occur simultaneously in the temperature rage 400–600 °C. From the work of Hornbogen & Jung (1964) one would only expect separation in the nucleation in the results of Fujii *et al.* (1968) for the 0.6 % atomic copper alloy aged at 500 °C. Close inspection of the results of the latter shows that this is so, but Fujii *et al.* (1968) have disguised the separation by drawing one broad peak through the yield-stress maxima. The two 'sets' of results are therefore entirely compatible and together they form an excellent description of the strengthening kinetics of copper-bearing alloys aged at temperatures in the range 400–600 °C.

However, our interest is in the behaviour of steels containing between 0.1 % and 0.4 % by mass of copper exposed at temperatures of *ca.* 350° and *ca.* 200 °C. The approximate ranges of temperature–ageing time appropriate to these high- and low-temperature exposures are indicated by the boxes included in figure 9. Clearly both areas lie outside the range covered by direct experimental information. The extrapolation of the t_p relation to low temperatures, shown by the broken set of parallel lines in figure 9 is our only guide to the strengthening kinetics of copper precipitation below 400 °C. The use of this extrapolation is only valid if, for the copper contents considered, we are well below the 'knee' of the appropriate 'C' curve for the ageing temperature in question.

At the temperature of the cold reactor exposures, *ca.* 200 °C, we may feel confident that the above condition holds, even for the lowest copper contents considered. At the temperature of the hot exposures the extrapolation may be valid for the highest atomic percentage of copper, 0.4 %, but it is unlikely to be so for the lowest. Schematic 'C' curves for copper contents of 0.4 % and 0.1 % by mass are included in figure 9. In §4.4 we show that there is some support for these curves in the observations made on the long-term aged steels. What is immediately clear from figure 9 is that these observations are broadly consistent with previous studies conducted at higher temperatures. The role of copper precipitation in the cold reactor exposures is much less clear. At the temperatures of exposure, *ca.* 170–220 °C, the extrapolation in figure 9 suggests that the times to peak strength will be *ca.* 10^4–10^7 years. Clearly, for copper precipitation to have a significant effect on yield stress under these conditions, there must be some mechanism for enhancement of the precipitation process. This will be discussed in §5.2.

4.2. *The dispersion strengthening of copper precipitates*

There is general agreement (Knowles & Kelly 1971; Russell & Brown 1972) that the mechanism responsible for the strengthening provided by a dispersion of copper precipitates is elastic modulus hardening. The model of Russell & Brown (1972) for the case of copper in ferrite gives a good account of the strength characteristics observed in iron–copper binary alloys.

In this system the obstacles are attractive to dislocations because $G_{Cu} < G_{Fe}$, where G is the shear modulus.

Russell & Brown (1972) derived the following equations for the increase in strength in ferrite containing copper precipitates with a mean planar radius, r.

$$\begin{aligned} \tau &= 0.8(Gb/L)\,(1-E_1^2/E_2^2)^{\frac{1}{2}}, \quad \arcsin E_1/E_2 \leqslant 50°; \\ \tau &= (Gb/L)\,(1-E_1^2/E_2^2)^{\frac{3}{4}}, \quad \arcsin E_1/E_2 \geqslant 50°. \end{aligned} \tag{9}$$

Here, τ is the shear stress, b is the Burgers vector and L is the obstacle spacing in the slip plane. The parameters E_1 and E_2 are the energies of a dislocation in copper and iron, respectively. Russell & Brown (1972) suggest the following relation for the ratio, E_1/E_2,

$$E_1/E_2 = 0.6 \ln (r/r_0)/\ln (R/r_0) + \ln (R/r)/\ln (R/r_0) \tag{10}$$

where $r_0 \approx 2.5b$ and $R \approx 1000\ r_0$.

The equations (9) and (10) predict a variation in yield stress with particle size which is illustrated in figure 10. Maximum strength is predicted when the particles are *ca.* 2.5 nm in diameter. This is in good agreement with the subsequent f.i.m. observations of Goodman *et al.* (1973).

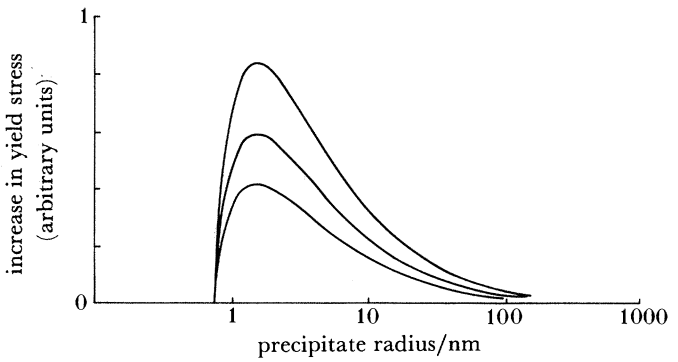

FIGURE 10. The calculated increase in yield stress as a function of precipitate size and volume fraction for a dispersion of copper particles in iron (after Russell & Brown 1972).

Russell & Brown (1972) show that the maximum increase in yield stress, $\Delta\sigma_y^{max}$, above the base ferrite value, is proportional to the root of the volume fraction of copper, f, in the alloy. In figure 11, the Fujii *et al.* (1968) data is plotted as a function of $f^{\frac{1}{2}}$. These data, then, suggest an expression for $\Delta\sigma_y^{max}$ as a function of volume fraction,

$$\Delta\sigma_y^{max} = [3.6 \times 10^3 (f^{\frac{1}{2}}) - 60]\ \text{MPa}. \tag{11}$$

To differentiate changes in yield stress from copper precipitation from those caused by damage loops we refer to $\Delta\sigma_y^{max}$ in subsequent sections as $\Delta\sigma_{Cu}^{max}$.

We can immediately use (11) to judge whether copper precipitation could account for the station 4 results shown in figure 3. At the irradiation temperature in this station the contribution to the yield stress from irradiation damage after 13 or 14 years of operation is relatively small. A figure of 10–15 MPa can be calculated approximately from the Barton *et al.* (1965) relation (4). In figure 12 the station 4 results after 13 or 14 years operation are plotted as a function of (copper content)$^{\frac{1}{2}}$ and compared with (11). The agreement is probably fortuitous,

PHILOSOPHICAL TRANSACTIONS OF THE ROYAL SOCIETY A MATHEMATICAL, PHYSICAL & ENGINEERING SCIENCES

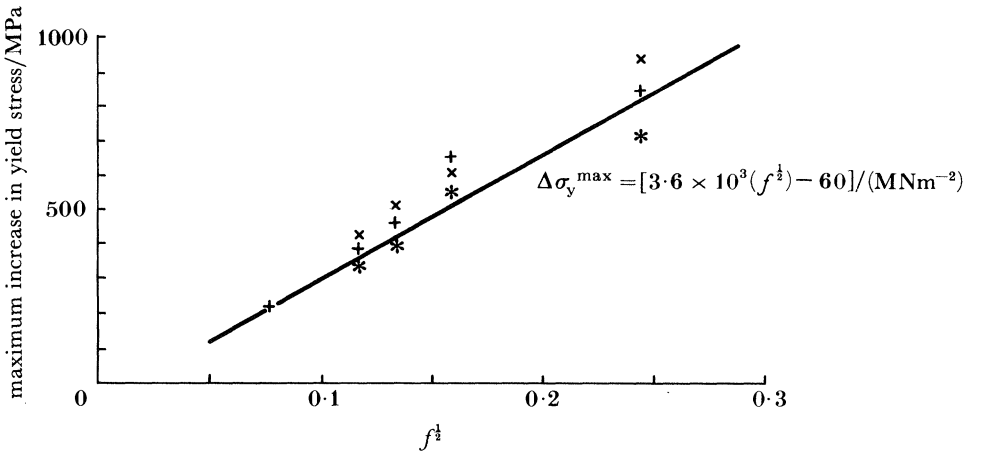

FIGURE 11. The maximum increase in yield stress, of iron–copper alloys aged at three temperatures, as a function of the square root of the volume fraction of copper (after Fujii *et al.* 1968). ×, 400 °C; +, 500 °C; *, 600 °C.

but the comparison does show that copper precipitation could be responsible for these results, if the precipitate dispersion were fully effective, i.e. the precipitate size was *ca.* 2.5 nm. This would also be consistent with our inability to resolve them in our microstructural study. It should be noted that in plotting the station 4 result for the manual weld in figure 12 we have corrected for the copper sulphide content in this particular material.

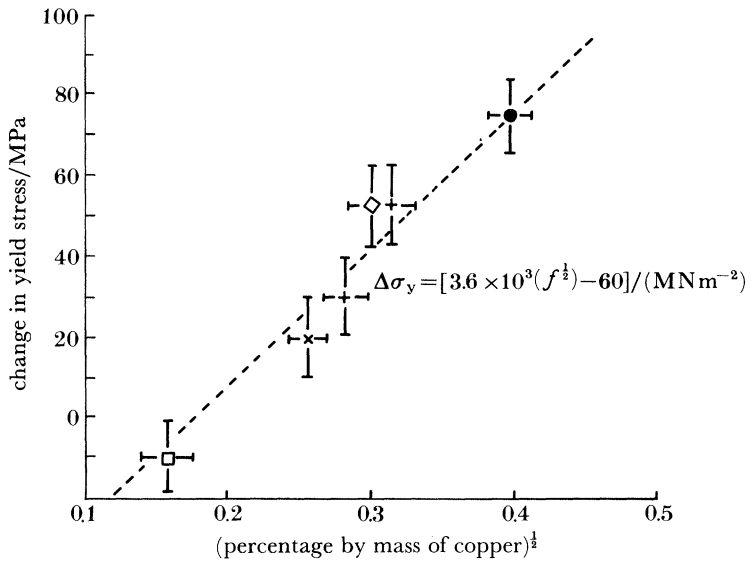

FIGURE 12. Change in yield stress of the 13 and 14 years' exposed tensile specimens from station 4 as a function of the square root of their copper contents. ●, machine weld; □, manual weld; ◇, plate; +, forging 1; ×, forging 2.

4.3. *The strengthening kinetics of copper precipitation*

The increment in yield stress, $\Delta\sigma_{Cu}$, arising from copper precipitation in a steel matrix will in general be a function of volume fraction, f, of copper in the steel, the ageing temperature, T_a, and time, t. Ideally we should determine this contribution to yield stress from a knowledge of the variation in precipitate radius, r, with these parameters and by combining this $r(t, T)$ with a theory that relates $\Delta\sigma_{Cu}$ to precipitate size and volume fraction (Russell & Brown 1972).

Analytical expressions do exist for the kinetics of precipitation both in the early stages (Ham 1958), and in the coarsening régime (Greenwood 1968). However, the derivation of these expressions involves making a number of simplifying assumptions and while they give a good qualitative description of the precipitation kinetics, quantitative analysis is confounded by a number of complicating features. This is particularly true for the system of copper in iron (Greenwood 1968).

We have obtained from a comparison of the Russell & Brown (1972) theory with the data of Fujii *et al.* (1968), a semi-empirical expression for $\Delta\sigma_{Cu}^{max}$ as a function of volume fraction of copper (equation (11)). We also have a semi-empirical prescription for determining t_p at any given ageing temperature. From an examination of existing data (Fujii *et al.* 1968; Krishnadev & Le May 1970) we find that (8) may be expressed as

$$\lg t_p = (1.1 \times 10^4)/T_a - 18.17, \tag{12}$$

where t_p is in years and T_a in kelvins. We can incorporate these relations to produce semi-empirical expressions for the time-dependence of the strength increase from copper precipitation in the following way.

Plots of the variation in strength with time in aged iron–copper alloys and steels containing copper have a characteristic form (figure 8). In general there are three distinct régimes of behaviour.

(i) For ageing times *ca.* $0 \leqslant t \leqslant \delta t_p (\delta < 1)$, where δ is apparently independent of volume fraction or t_p, $\Delta\sigma_{Cu} = 0$.

(ii) For ageing times *ca.* $\delta t_p \leqslant t \leqslant t_p$, $\Delta\sigma_{Cu}$ increases with time to a maximum of $\Delta\sigma_{Cu}^{max}$ at $t = t_p$. The rise in $\Delta\sigma_{Cu}$ is approximately linear in $\lg t$. This is most noticeable in the experimental results of Krishnadev & Le May (1970).

(iii) For ageing times *ca.* $t_p \leqslant t \leqslant Nt_p$, $\Delta\sigma_{Cu}$ decreases linearly with $\lg t$ from $\Delta\sigma_{Cu}^{max}$ at $t = t_p$, to a given fraction of this maximum value at $t = Nt_p$. If we take the fraction as $\frac{1}{2}\Delta\sigma_{Cu}^{max}$, then $N \approx 10$. Again, N is approximately independent of t_p and volume fraction.

An examination of simple precipitate growth models, combined with the equations (9) and (10) of Russell & Brown (1972), provides considerable mechanistic support for these empirical observations (Fisher *et al.* 1984*c*). In our model we use the above observations together with our expressions for $\Delta\sigma_{Cu}^{max}$ and t_p to provide the following semi-empirical description of the copper contribution to strength in our Magnox steels.

$$\left.\begin{array}{ll} \text{(i)} & \text{For } t < 0.05t_p; \Delta\sigma_{Cu} = 0. \\ \text{(ii)} & \text{For } 0.05t_p \leqslant t \leqslant t_p; \Delta\sigma_{Cu} = 0.77 \lg (t/0.05t_p)\, \Delta\sigma_{Cu}^{max}. \\ \text{(iii)} & \text{For } t > t_p; \Delta\sigma_{Cu} = -0.5 \lg (0.01t/t_p)\, \Delta\sigma_{Cu}^{max}. \end{array}\right\} \tag{13}$$

This description is compared with the data of Krishnadev & Le May (1970) in figure 13.

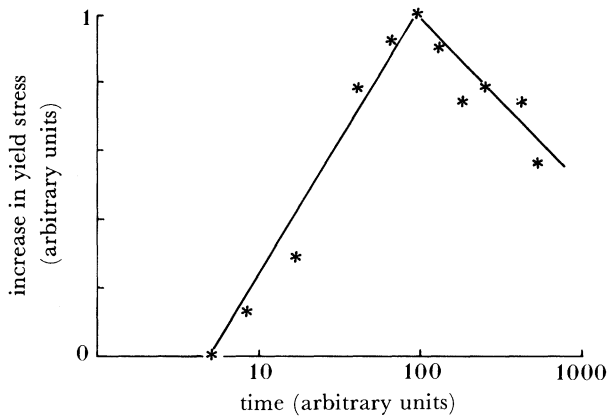

FIGURE 13. The expressions for the time-dependence of the copper contribution to yield stress used in the model compared with the data of Krishnadev & Le May (1970) at 500 °C.

4.4 *Comparison with our long-term ageing results*

From the above expressions we may compute $\Delta\sigma_{Cu}(t)$ at any ageing temperature T_a, provided that the precipitation process is diffusion-limited. Furthermore, by using the form of the Russell & Brown (1972) equations (9) and (10), which yield $\Delta\sigma_{Cu}(r)$ (figure 10), we can approximately determine $r(t)$ when $t > t_p$ if we assume that the full volume fraction of copper has precipitated. In figure 14, $\Delta\sigma_{Cu}(t)$ and $r(t)$ are plotted for a 0.4 % by mass of copper steel, aged at 355 °C. At this temperature the computed values $\Delta\sigma_{Cu} \approx 74$ MPa and precipitate radius ≈ 7 nm at $t = 19600$ h, correspond most closely to our experimental measurements. The latter provide support, therefore, not only for the Russell & Brown (1972) theory, but also for the use of our empirical relations (13).

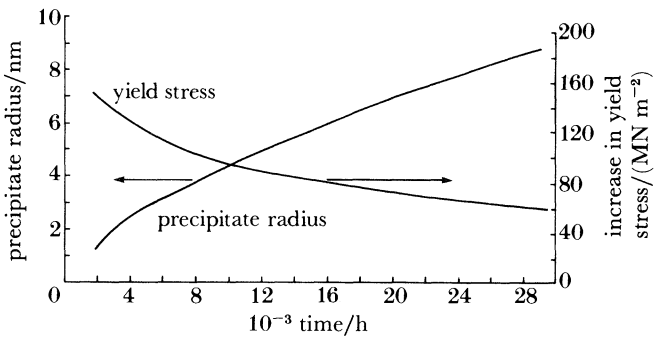

FIGURE 14. The calculated values of yield stress increase and precipitate radius as a function of ageing time for a 0.4 % by mass of copper steel aged at 355 °C.

The fact that the above analysis may be satisfactorily performed for the high-copper steel (steel I), confirms that for a steel of this composition, aged at *ca.* 350 °C, the precipitation is diffusion-controlled and occurs on both dislocations and matrix (see schematic 'C' curve in figure 9). No comparable analysis can be done for the aged low-copper steel (steel II). In this steel, aged at *ca.* 350 °C, nucleation was observed only on dislocations (in agreement with the

corresponding schematic 'C' curves) and less than half of the available volume fraction was precipitated. In this instance one would expect any increase in strength to be minimal. This was confirmed by a subsequent comparison of hardness measurements made on control and aged specimens of this material (Fisher *et al.* 1984*b*).

4.5. *The high-temperature Magnox exposures*

In the station 3 hot locations, the steels I and II were exposed at 390 °C for the initial six years of operation. At this temperature the precipitation of copper in steels containing only *ca.* 0.1 % by mass of this element, will be even further into the nucleation-controlled régime than at *ca.* 350 °C. We might therefore expect any resultant changes in yield stress, as in our long-term aged sample, to be negligible. In the steel containing 0.4 % by mass of copper (steel I), however, we expect nucleation of copper to occur both on dislocations and within the matrix, producing a peak increase in strength after *ca.* 1000 h at 390 °C (figure 9). If we use this value for t_p in (13) we can compute $\Delta\sigma_{Cu}(t)$ for this case. We find, after 2 years of exposure, the estimated increase is *ca.* 65 MPa; after 3 a, *ca.* 52 MPa. These figures are to be compared with the monitoring measurements, shown in figure 2, of 60 and 59 MPa, respectively.

While we have clearly established an interpretation for the Magnox hot exposures, the monitoring results at low irradiation temperatures require further detailed investigation. We have shown that, at least for the station 4 data, the increases in yield stress could arise from copper precipitation, but we have yet to show that precipitation to maximum effect could occur within the actual periods of exposure. In the following section we demonstrate that the required enhancement of the precipitation process arises from the production of mobile vacancies in the irradiated steels.

5. Formulation of the model

Under the conditions of irradiation listed in table 5, the primary form of radiation damage is thought to consist of small (less than 2 nm diameter) interstitial or vacancy loops (or both) (Little & Harries 1970). These features arise from the collapse of defect clusters formed in the displacement spike (Barton *et al.* 1965).

Only *ca.* 12 % of the vacancies produced in a nascent cascade survive to become mobile monovacancies (Odette 1979). These may give rise to a small but significant vacancy supersaturation at these low temperatures. The absence of a flux-dependence of radiation hardening (Barton *et al.* 1965) indicates that the nucleation of the damage loops is not controlled by the diffusion of the mobile point defects but is only dependent on the number of clusters formed as a result of the initial displacement spikes.

In our model we assume that there are, in general, two contributions to the radiation hardening of pressure-vessel steels under irradiation; (i) the contribution from irradiation damage loops and (ii) the contribution from copper precipitation, which may be enhanced through the production of mobile monovacancies.

For our hot Magnox exposures, (i) is negligible and (ii) is not enhanced by irradiation. For the cold exposures (i) may be significant, particularly in steels low in aluminium and irradiated at the lowest temperatures; (ii) may or may not be significant depending on copper content and the irradiating flux.

5.1. *The contribution from damage clusters*

At irradiation temperatures in the range appropriate to the 'cold' Magnox exposures (170–225 °C), nitrogen has a profound influence on the formation and stability of the damage loops (Little & Harries 1970). Elements that can remove 'free' nitrogen as nitrides are therefore important constituents of mild steels in respect of their radiation sensitivity. Any calculation of the yield-strength increase from irradiation damage loops must therefore include the influence of the elements aluminium and silicon. The role of these elements in forming stable nitrides during heat treatment before irradiation was confirmed by our microstructural studies.

At first sight it would appear that the relation (4) found by Barton *et al.* (1965) could be used directly to calculate the damage-loop contribution in the Magnox steels. Certainly it is simple enough to assign a value for A in (4) for each of the Magnox cases of interest, because A only depends on temperature and composition and these are relatively well established parameters. The selected values for A for the plate and weld steels are included in tables 6 and 7, respectively.

However, there are two complications that require resolution before the use of equation (4) of Barton *et al.* (1965).

(i) The steels used by Barton *et al.* (1965) contained significant concentrations of copper (0.13 %–0.18 % by mass). We must therefore demonstrate that under their irradiation conditions the copper did not precipitate sufficiently to make any contribution to the measured change in yield stress.

(ii) The irradiations of Barton *et al.* (1965) were performed in a hollow fuel-element position in PLUTO. We must, therefore, make some adjustment for the influence of the neutron spectrum in deriving a value for $\Delta\sigma_{\mathrm{dam}}$, the damage-loop contribution to hardening, relevant to Magnox exposures.

In respect of (i), we may compare the results of Barton *et al.* (1965) with those from Tokaku *et al.* (1979). These workers irradiated pure iron to *ca.* 5×10^{18} neutrons cm^{-2} at 250 °C and found an increase in yield strength of *ca.* 64 MPa. From (4) it was found that these figures correspond to a value of $A\approx4.1$. This compares with the value found by Barton *et al.* (1965) in aluminium-killed steel, irradiated at 250 °C, of *ca.* 4.5 (±1). This comparison suggests that the influence of copper in the Barton *et al.* (1965) experiments was not significant. This is a result of the very short times of the irradiations employed (Fisher *et al.* 1984*c*). It is also evident that the radiation sensitivity of aluminium-killed steel approaches that of pure iron.

With regard to (ii), clearly we must include an additional parameter in (4) to account for the differences in spectra between the fuel-element location in PLUTO and the below- and side-core locations in our Magnox reactors. A component receiving the same integrated fission dose, $\phi_{\mathrm{f}}t$, in these spectra will not suffer the same damaging effects. For use in Magnox calculations, (4) must be modified to a form

$$\Delta\sigma_{\mathrm{dam}}(t)=A[\alpha_{\mathrm{b,s}}(\phi_{\mathrm{f}}t)]^{\frac{1}{2}}, \tag{14}$$

where the parameters $\alpha_{\mathrm{b}},\alpha_{\mathrm{s}}(\alpha_{\mathrm{b}}\neq\alpha_{\mathrm{s}})$ refer to the below- and side-core locations, respectively, and reflect the equivalent damaging doses in these locations compared with those in the relevant positions in PLUTO.

Because of the uncertainties surrounding our knowledge of the appropriate cross section for damage loop formation and our incomplete knowledge of the Magnox spectra, theoretical

estimates of suitable values for $\alpha_{b,s}$ are very crude (Fisher *et al.* 1984*c*). We found a rather broad range of values for α_b of *ca.* $2 \rightarrow 5$ and α_s of *ca.* $0.5 \rightarrow 1.5$. More precise values were established by making a comparison of (4) with the plate monitoring results from station 2. These data are plentiful and are obtained on a steel with relatively low contents of aluminium and copper. In addition to these factors, the dose rates in this station are the highest considered; the changes in yield stress are therefore dominated by the damage loop contribution. Values for $\alpha_{b,s}$ of *ca.* 3 and 1 were determined in this way. These values were used throughout the modelling computations.

5.2. *The copper contribution under irradiation*

We have formulated a prescription for the calculation of the strengthening from a dispersion of copper precipitates as a function of time, $\Delta\sigma_{Cu}(t)$, in the absence of irradiation. We need to determine this contribution under irradiation.

Early experiments (Hornbogen & Glenn 1960) on copper precipitate growth in quenched iron–copper alloys showed that, in the early stages of precipitation, quenched-in vacancies gave an enhancement of the rate of copper atom diffusion. The initial enhancement in diffusion coefficient was determined as

$$D_E = D_{T_1}(C_v^{T_2}/C_v^{T_1}); \quad C_v^T = \exp(-E_v^f/kT), \tag{15}$$

where D_E is the enhanced diffusion coefficient; D_{T_1}, the 'normal' coefficient at the ageing temperature, T_1, and T_2, the quenching temperature; E_v^f is the energy of formation of a vacancy. The enhancement in diffusion was found to decrease as the excess vacancy concentration decayed.

Under irradiation a steady-state concentration of vacancies, C_v^{irr}, is produced. For the conditions of the Magnox exposures, C_v^{irr} may be calculated from the equation

$$C_v^{irr} = K_v/D_v k_v^2, \tag{16}$$

where K_v is the production rate of mobile monovacancies and D_v is the appropriate vacancy diffusivity. The parameter, k_v^2, is given by

$$k_v^2 = Z_v \rho_d, \tag{17}$$

where ρ_d is the dislocation density and $Z_v \approx 2$. The vacancy production rate, K_v, is determined for the Magnox exposures from a knowledge of the atomic displacement rates for the locations of interest and a comparison of the cross sections for atomic displacement and mobile vacancy production (Odette 1970; Fisher *et al.* 1984*c*).

From C_v^{irr}, an enhanced diffusion coefficient for copper-atom diffusion, D_{irr}, may be calculated from the relation

$$D_{irr} = D_T(C_v^{irr}/C_v^T), \tag{18}$$

where D_T is the appropriate diffusion coefficient at the temperature T, in the absence of irradiation.

The precipitate radius at any time may be written, $r(t) = g(Dt)$, where D is the appropriate diffusion coefficient. For purely *thermal* diffusion, at a temperature T, we may write

$$r_c = g(D_T t_p), \tag{19}$$

Table 6. Model parameters for the plate steels

station (location)	irradiation temperature/°C	fission flux / $cm^{-2}\ s^{-1}$	Barton constant, A	t_p/a	t'_p/a	$\Delta\sigma_{Cu}^{max}$/MPa
1	167	10^7	12	6.7×10^6	267	57
2 (1)	190	8.1×10^8	10.5	3.9×10^5	4.7	23
2 (2)	190	1.6×10^9	10.5	3.9×10^5	8.9	23
3 (1)	170	4.4×10^7	7	4.6×10^6	64	154
3 (2)	170	1.7×10^7	7	4.6×10^6	165	154
4	225	3.8×10^8	3.5	8.3×10^3	15	41
5 (1)	221	5.8×10^8	5.5	1.3×10^4	36	57
5 (2)	190	1.5×10^8	6.5	3.9×10^5	26	57

Table 7. Model parameters for the weld steels

station (location)	irradiation temperature/°C	fission flux / $cm^{-2}\ s^{-1}$	Barton constant, A	t_p/a	t'_p/a	$\Delta\sigma_{Cu}^{max}$/MPa
1	167	10^7	12	6.7×10^6	890	91
2 (1)	190	8.1×10^8	11	3.9×10^5	16	91
2 (2)	190	1.6×10^9	11	3.9×10^5	30	91
3	170	4.4×10^7	12	4.6×10^6	216	91
4	225	3.8×10^8	8.5	8.3×10^3	50	75

where r_c is the critical precipitate radius at peak strength after the time t_p. Under irradiation, at the same temperature, the critical size will be reached in a time, t'_p, given by

$$t'_p = t_p(D_T/D_{irr}) = t_p(C_v^T/C_v^{irr}). \tag{20}$$

The values of t'_p for the plate steels irradiated in cold Magnox locations are shown in table 6, together with the appropriate values of $\Delta\sigma_{Cu}^{max}$. Table 7 shows the corresponding values of t'_p for the weld steels irradiated in the cold locations, again with appropriate values of $\Delta\sigma_{Cu}^{max}$. Clearly, in most stations, copper precipitation will make a significant contribution to changes in the yield stress in both plate and welds at sometime during the lifetimes of the vessels. Note, however, that in no location is t'_p much less than the lifetime of the vessel. We might expect, then, that the copper precipitates will remain below the limit of resolution of transmission microscopy in the steels irradiated in cold locations. This is certainly true for the steels in station 4 after 13–14 years of operation, in accordance with our microstructural studies.

To obtain suitable expressions for $\Delta\sigma_{Cu}(t)$ we simply substitute t'_p for t_p in (13).

6. Superposition of the two contributions

The effective shear stress, τ_k, available for pushing dislocations through short-range obstacles in the presence of long-range internal stresses arising from dislocation networks, is given by Diehl & Seidel (1969),

$$\tau_a - \tau_{LR} = \tau_k. \tag{21}$$

Here, τ_a is the applied stress and τ_{LR} the stress necessary for moving dislocations through the long-range stress field.

In the case we are considering, we have two types of short-range obstacle, copper precipitates and damage loops. We must determine the relative strengths and spacings of these obstacles to enable us to combine their separate effects.

6.1. *The strength and spacing of the copper precipitates*

From the equations (9) and (10) of Russell & Brown (1972) we may derive an approximate expression for the increase in strength arising from a given size and volume fraction of copper precipitate, in the absence of any other obstacles to dislocation motion.

Under the conditions of interest in the Magnox low-temperature exposures, the copper precipitates are below or just above the critical size, r_c. When $r \sim r_c$, the increase in shear stress arising from the precipitates alone would be

$$\tau_{Cu} \approx 0.1Gb/L. \tag{22}$$

The strength of the individual copper precipitates is therefore *ca.* 10–12% of the Orowan strength. The Orowan stress arising from obstacles of spacing L is $0.8\ Gb/L$.

We may determine the copper precipitate spacing from the relation (Russell & Brown 1972)

$$L^{-1} = f^{\frac{1}{2}}/1.77r. \tag{23}$$

For our steels we find $L \approx 35$–90 nm, depending on f.

6.2. *The strength and spacing of the damage loops*

The increase in shear stress arising from a dispersion of defect loops of spacing L is given by (Bement 1970)

$$\tau_{dam} = Gb/\beta L, \tag{24}$$

where $\beta \approx 3$–4 (Bement 1970).

Damage loops therefore have a strength *ca.* 30–35% of the Orowan strength. From the changes in $\Delta\sigma_{dam}$ predicted by equation (4) of Barton *et al.* (1965) for our conditions, we can calculate approximately the minimum loop spacing with the use of (24). We find that $L \approx 200$–300 nm is the minimum spacing likely to occur under the conditions we consider.

6.3. *The appropriate superposition*

If F_{loop} and F_{prec} are the respective strengths of individual damage loops and precipitates, it follows from the two previous sections that we require the superposition of the effects of two types of short-range obstacle where,

$$F_{loop} \gg F_{prec} \quad \text{and} \quad L_{loop} \gg L_{prec}.$$

For this situation, the appropriate combination of the individual shear stresses is by simple linear addition (Diehl & Seidel 1969) so that

$$\tau_{tot} = \tau_{dam} + \tau_{Cu}, \tag{25}$$

where τ_{tot} is the resultant increase in shear stress arising from the combination. It immediately follows that the overall increase in yield stress as a result of the formation of both precipitates and damage loops is given by,

$$\Delta\sigma_{tot} = \Delta\sigma_{dam} + \Delta\sigma_{Cu}, \tag{26}$$

where $\Delta\sigma_{dam}$ and $\Delta\sigma_{Cu}$ are the respective individual contributions from loops and precipitates.

With $\Delta\sigma_{dam}(t)$ from (14) and $\Delta\sigma_{Cu}(t)$ from (13), with t_p replaced by t'_p, we may calculate $\Delta\sigma_{tot}(t)$ for all steels, both plate and weld, in the 'cold' Magnox locations. The results of these computations are compared with the monitoring data in the next section.

7. Results of the model

The particular values taken for the various parameters in the model are either listed in the tables or given in the text. The accuracy of the measured copper contents, with the exception of those in station 4, are thought to be no better than $\pm 20\,\%$. In practice we make little use of this flexibility in the calculations. For the steel plate in station 5 we use a content of *ca.* $0.12\,\%$ by mass rather than the quoted $0.15\,\%$. For all the weld steels we use a content of *ca.* $0.2\,\%$ by mass with the exception of station 4 where we use our measured value of $0.16\,\%$.

The values of the Barton *et al.* (1965) constant A chosen for the welds (table 7) are appropriate for each particular irradiation temperature, with the assumption that all the weld metals behave as silicon-killed steels in respect of nitrogen content. This assumption is supported by our observations that stress-relieved welds only contain the silicon–manganese nitride, (Si, Mn) N and no aluminium nitride. The three features that distinguish welds from plate steels in the model are therefore the value assigned to the constant A, the higher dislocation density, and the generally higher copper content.

Measured values for the activation energy for copper diffusion in iron lie within the range $2.5 \pm (0.05)$ eV (Salje & Feller-Kniepmeier 1977). This is similar to the activation energy for self-diffusion, and we assume that this energy corresponds to the sum of energies for vacancy formation and migration $(E_{\mathrm{v}}^{\mathrm{f}} + E_{\mathrm{v}}^{\mathrm{m}})$. From equations (16) and (20), the reduced time to the peak, t'_{p}, may be written

$$t'_{\mathrm{p}} = t_{\mathrm{p}}\,[k_{\mathrm{v}}^2 \exp -(E_{\mathrm{v}}^{\mathrm{m}} + E_{\mathrm{v}}^{\mathrm{f}})/kT_{\mathrm{irr}}]/K_{\mathrm{v}}. \tag{27}$$

It follows immediately that the individual values assigned to $E_{\mathrm{v}}^{\mathrm{m}}$ and $E_{\mathrm{v}}^{\mathrm{f}}$ have no influence on t'_{p}, provided their sum is fixed. Increasing $(E_{\mathrm{v}}^{\mathrm{m}} + E_{\mathrm{v}}^{\mathrm{f}})$, or K_{v}, reduces t'_{p}. The values computed for t'_{p} shown in tables 6 and 7 were obtained with $(E_{\mathrm{v}}^{\mathrm{m}} + E_{\mathrm{v}}^{\mathrm{f}}) = 2.44$ eV, i.e. the lower end of the measured range. Similar values for t'_{p} can be found by using an activation energy at the upper end of the range, provided there is a suitable and corresponding reduction in the vacancy production rate. The absolute levels of t'_{p} used in the model can therefore be obtained from a useful range of acceptable values for activation energy and defect production rate. However, the *relative* values of t'_{p} between stations and locations arise principally from the relative magnitudes of the neutron flux. It is these figures that are ultimately responsible for the successful interpretation of the data from locations with widely different conditions of exposure.

7.1. *Results for plate steels*

The model calculations are compared with the monitoring measurements in figure 15. In each graph, both $\Delta\sigma_{\mathrm{tot}}(t)$ (solid line) and $\Delta\sigma_{\mathrm{Cu}}(t)$ (broken line) are displayed. In this way the full significance of copper precipitation may be appreciated.

(i) *Station* 1

The monitoring samples in this station contain less than $0.01\,\%$ by mass of aluminium and have a relatively high copper content ($0.12\,\%$ by mass). They are therefore potentially susceptible to both damage loop formation and copper precipitation. However, the neutron flux in this instance is the lowest of the stations considered. The copper contribution to the yield stress is less than 10 MPa even after 25 years of operation. Notwithstanding the negligible aluminium content and low irradiation temperature, the damage loop contribution is also small throughout the reactor lifetime; again this is a consequence of the very low neutron flux.

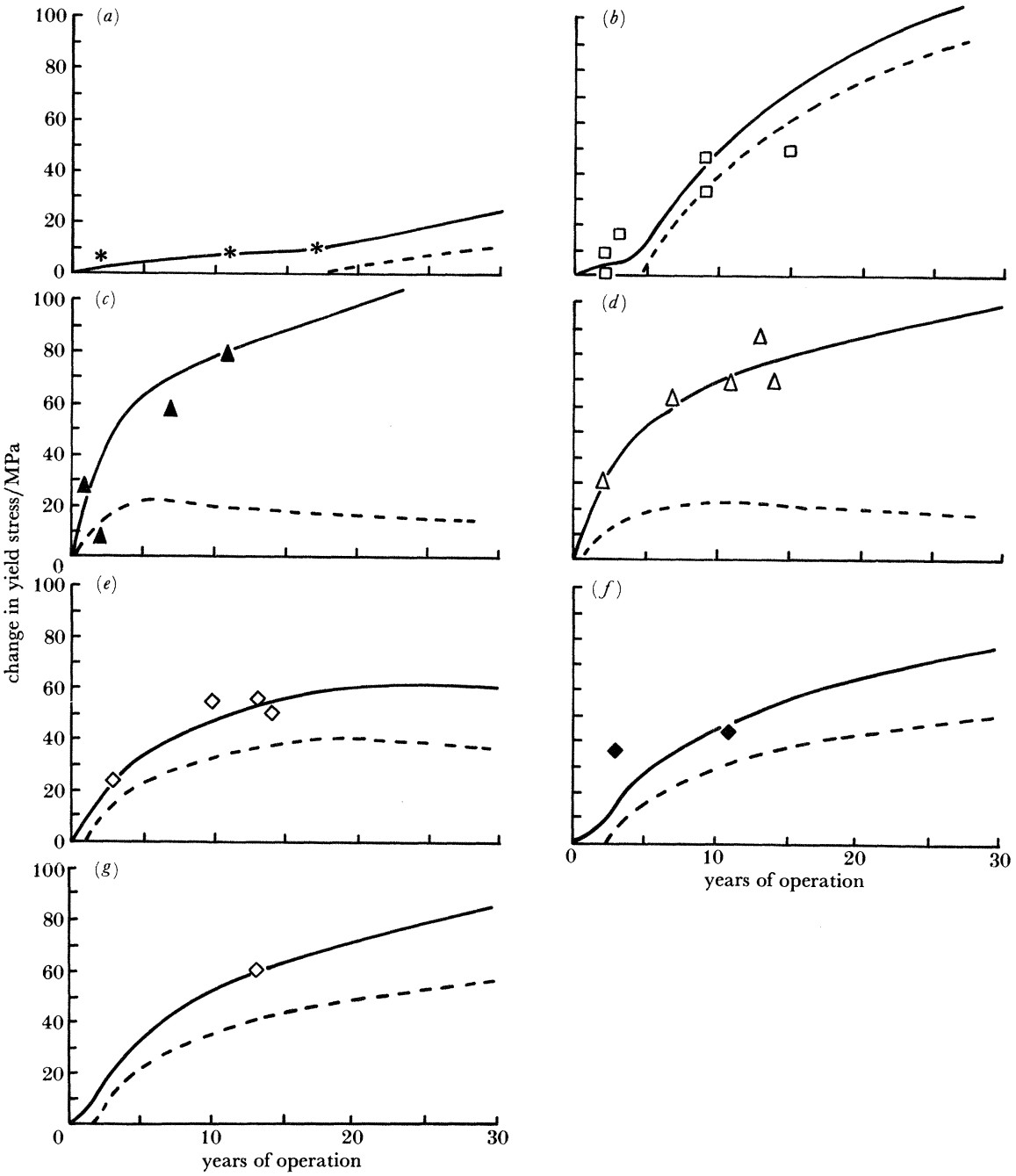

FIGURE 15. Computed increase in yield stress compared with experimental data for plate steels. The broken lines show the contribution from copper precipitates. (*a*) Station 1 (170 °C); (*b*) station 3 (170 °C); (*c*) station 2(1) (190 °C); (*d*) station 2(2) (190 °C); (*e*) station 4 (225 °C); (*f*) station 5(1) (221 °C); (*g*) station 5(2) (190 °C).

(ii) *Station 2*

The steels exposed in this station contain *ca.* 0.008 % by mass of aluminium and *ca.* 0.06 % by mass of copper. The neutron fluxes in the two locations of interest are the highest of all those considered. The copper contribution reaches its peak rapidly under the high flux, but the main contribution to yield stress comes from the damage loops. The yield stress may rise by *ca.* 100 MPa in this plate steel over the lifetime of the station.

(iii) *Station* 3

The levels of flux at the two 'cold' locations in this station are only slightly above that for station 1, and the steel exposed has a significantly higher aluminium content *ca.* 0.018% by mass. The increase in strength from damage loop formation is therefore negligible (less than *ca.* 10 MPa), even after 20 years of operation.

There are sufficient data from the two locations to demonstrate that the measured increases are much larger than this figure, reaching *ca.* 40 MPa, after only 10 years of operation.

Because of the uncertainty (*ca.* two times) in flux measurement for location 2, and the similarity of the data from this location with those from location 1, the model results in the figure have been computed by using an intermediate flux level *ca.* 3.5×10^7 neutrons cm^{-2} s^{-1}, which is twice that estimated for location 2, but corresponds approximately with that measured for location 1. These computed curves are sufficient to show clearly that the monitoring results arise almost entirely from the onset of copper precipitation in a steel containing a very high (0.4% by mass) copper content.

(iv) *Station* 4

The plate steel exposed in station 4 has a high aluminium content, *ca.* 0.05% by mass, with a copper level *ca.* 0.09% by mass. The neutron flux is relatively high and produces a peak in $\Delta\sigma_{Cu}$ after *ca.* 17 years of operation. The high aluminium content, allied to the high irradiation temperature, 225 °C, minimizes the contribution from $\Delta\sigma_{dam}$. The monitoring data for this station suggest that the yield stress may be saturating in the plate steel. This suggestion is reinforced by the measurements made on forgings exposed under identical conditions (figure 3). The results of the model show that this saturation arises from the early peak in $\Delta\sigma_{Cu}$ which dominates the increase in strength.

(v) *Station* 5

The parameters relevant to the two locations in this station are similar to those for station 4. The neutron flux levels produce peaks in $\Delta\sigma_{Cu}$ after *ca.* 30 years of operation. Both the copper and aluminium levels are relatively high in the monitoring steel. The change in yield stress is therefore dominated by copper precipitation. Unfortunately there are only three data points from the monitoring scheme for this station.

7.2 *Results for weld steels*

The model calculations are compared with the monitoring data for the weld steels in figure 16.

(i) *Station* 1

For this station, with its low neutron flux, the influence of the higher dislocation density in the welds, compared with the plate steels, is such that there is no contribution from $\Delta\sigma_{Cu}$ within the lifetime of the vessel. Our lack of compositional analysis for this material is therefore no handicap to making a firm prediction of the negligible change in properties.

(ii) *Station* 2

The effect of the high dislocation density of the welds is demonstrated most clearly in the results from this station. The peak contributions from copper are postponed to *ca.* 20–30 years

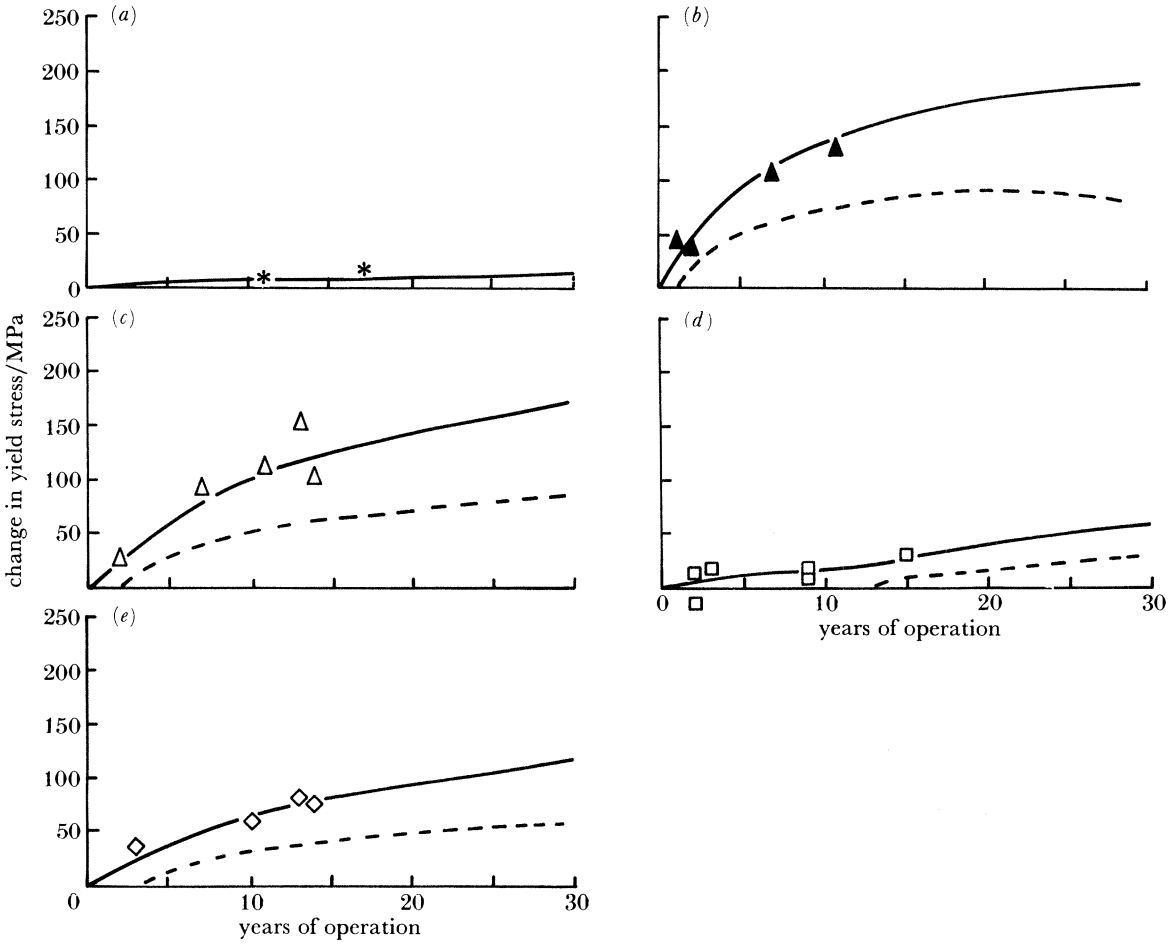

FIGURE 16. Computed increase in yield stress compared with experimental data for weld steels. The broken lines show the contribution from copper precipitates. (*a*) Station 1 (170 °C); (*b*) station 2(1) (190 °C); (*c*) station 2(2) (190 °C); (*d*) station 3 (170 °C); (*e*) station 4 (225 °C).

and the combination of high copper content and high flux leads to a significant increase in yield stress that increases throughout the lifetime of the vessel. After 30 years of operation the increase in yield stress may approach 200 MPa.

(iii) *Station* 3

In a similar way to our management of the plate steel analysis for this station, we treat the data from both locations as arising from location 1 and use the appropriate parameters in the model. Compared with the plate steel, the contribution from copper is reduced in magnitude and delayed. Overall the changes in yield stress in this instance are not expected to exceed *ca.* 50 MPa over the lifetime of the station.

(iv) *Station* 4

Unlike the plate steel results for this station, which show a saturation in yield stress after *ca.* 15 years of operation, the weld prediction continues to rise throughout the vessel lifetime.

This is a consequence of the higher dislocation density in the weld, which postpones the copper peak, and the more significant contribution from damage loops. After 30 years of operation the yield stress may rise by *ca.* 120 MPa in the weld steel in this station.

8. Discussion

The model gives an entirely satisfactory interpretation of the yield-stress data from both plate and weld steels exposed in the Magnox monitoring scheme. These data are obtained from steels with a wide variation in composition, exposed under a variety of conditions.

While the weld steels generally have a significantly higher copper content than the corresponding plate steels, the influence of this content is offset, in the two 'low-flux' stations, 1 and 3, by the high dislocation density in the welds. In only two stations, 4 and 5, do the effects of copper content and dislocation density combine to produce a significant increase in yield stress that increases throughout the years of operation.

Direct experimental evidence in support of the model, in terms of the observation of copper precipitates in the 'low-temperature' exposed steels, is unlikely to come from transmission microscopy. Even after 20 years of operation in station 2, the precipitates in the plate steels are not expected to exceed *ca.* 6 nm in diameter. Experimental support for the model must therefore come from the application of alternative techniques.

A brief outline of the model was first given at the British Nuclear Energy Society Conference at Brighton in April 1983 (Fisher *et al.* 1984*a*). At the same meeting Frisius *et al.* (1983) presented evidence for the formation of small copper precipitates in iron–copper alloys, irradiated at 290 °C. The particles were detected by using small-angle neutron scattering (s.a.n.s.). The same technique has been applied to our own Magnox steels by Jones & Buswell (1984) and their preliminary results do provide support for our model.

One particularly interesting feature of the model lies in its potential application for the interpretation of the behaviour of p.w.r. pressure-vessel steels. At irradiation temperatures *ca.* 290 °C, $\Delta\sigma_{\mathrm{dam}} \ll \Delta\sigma_{\mathrm{Cu}}$ in steels with copper contents greater than *ca.* 0.2 % by mass. The older U.S. steels, with copper contents ranging from 0.2–0.5 % by mass, showed substantial increases in strength under irradiation, with a corresponding rise in the transition temperature (Potapovs & Hawthorne 1969). Our model suggests that the formation of copper precipitates was principally responsible for these changes. The data from these U.S. steels should be particularly amenable to interpretation in terms of the irradiation-enhanced precipitation of copper. It is gratifying to note that such an interpretation was reported very recently (Odette & Lombrozo 1983), just after the Brighton Conference.

9. Conclusions

(i) The yield-stress measurements made on plate and weld steel specimens exposed in the Magnox monitoring scheme have been successfully interpreted.

(ii) The model employed for the interpretation assumes that, in general, the strengthening effect of irradiation damage loops is augmented by the precipitation of a fine dispersion of copper particles within the steel matrix.

(iii) In steels exposed at high temperatures (greater than *ca.* 340 °C), the contribution to strength from damage loops is negligible. There is no enhancement in copper precipitation from

irradiation, and significant hardening is only found in steels with a high copper content where the temperature of exposure is sufficiently below the solubility temperature to ensure that the precipitation is diffusion-controlled. Under these conditions of high-temperature exposure diffusion is sufficiently rapid to allow overageing of the copper precipitates.

(iv) In steels exposed at low temperatures (170–225 °C), both damage loops and copper precipitates may contribute to an increase in strength. The precipitation of copper is enhanced by irradiation. While the particles may have a profound influence on dislocation mobility they remain below the resolution limit of transmission microscopy throughout the lifetime of any Magnox station.

(v) Experimental evidence for the irradiation-enhanced precipitation of copper in iron–copper alloys has come from overseas s.a.n.s. studies. Preliminary work, using the same technique on the Magnox steels, has also given some support to the model.

(vi) The model suggests that the yield-stress changes in high-copper steels irradiated under p.w.r. conditions should be dominated by the contribution from copper precipitates. A similar model (Odette & Lombrozo 1983), independently formulated, is now being used successfully for the interpretation of data from U.S. p.w.r. pressure-vessel steels.

This paper is published by permission of the Central Electricity Generating Board. The authors express their gratitude to Dr R. B. Jones (Berkeley Nuclear Laboratories) and Dr W. Charnock (C.E.G.B., North Western Region Scientific Services Department) for their generous assistance and advice throughout the formulation of this work.

References

Barton, P. J., Harries, D. R. & Mogford, I. L. 1965 Effects of neutron dose rate and irradiation temperature on hardening. *J. Iron Steel Inst.* **203**, 507–510.

Bement, A. L. 1970 Fundamental materials problems in reactors. In *Proceedings of Second International Conference on Strength of Metals and Alloys, Pacific Grove, California*, vol. 2, pp. 693–728. U.S.A.: ASM.

Burke, J. 1965 Precipitation kinetics. In *The kinetics of phase transformations in metals*, p. 55. Oxford: Pergamon Press.

Cottrell, A. H. 1961 Theoretical aspects of radiation damage and brittle fracture. In *Steels for reactor pressure circuits* pp. 281–296. London and Bradford: Lund Humphries.

Diehl, J. & Siedel, G. P. 1969 Effect of alloying and cold work on embrittlement. In *Proceedings of Symposium on Radiation Damage in Reactor Materials at Vienna*, pp. 187–212. Vienna: IAEA.

Fisher, S. B., Harbottle, J. E. & Aldridge, N. 1982 Characterisation of precipitates in mild steels. Central Electricity Generating Board Report no. TPRD/B/0108/N82.

Fisher, S. B., Harbottle, J. E. & Aldridge, N. 1984*a* Microstructure related to irradiation hardening. In *Proceedings of Conference on Dimensional Stability and Mechanical Behaviour of Irradiated Metals and Alloys at Brighton, April* 1983, vol. 2, pp. 87–92. London: BNES.

Fisher, S. B., Aldridge, N. & Harbottle, J. E. 1984*b* Examination of long-term aged steels. Central Electricity Generating Board Report no. TPRD/B/0397/N84.

Fisher, S. B., Harbottle, J. E. & Aldridge, N. 1984*c* Model for hardening of Magnox steels. Central Electricity Generating Board Report no. TPRD/B/0398/N84.

Frisius, F. & Bünemann, D. 1979 The measurement of radiation defects in iron alloys by means of small angle neutron scattering. In *Proceedings of Conference on Irradiation Behaviour of Metallic Materials for Fast Reactor Core Components* (ed. J. Poirier & J. M. Dupouy), pp. 247–251. France: CEA.

Frisius, F., Kampmann, R., Beavan, P. A. & Wagner, R. 1983 Influence of copper on defect structure and radiation strengthening of iron. In *Proceedings of Conference on Dimensional Stability and Mechanical Behaviour of Irradiated Metals and Alloys, Brighton, April* 1983, vol. 1, pp. 171–174. London: BNES.

Fujii, A., Nemoto, M., Suto, H. & Monma, K. 1968 Precipitation hardening in iron-copper alloys. *Trans. Japan Inst. Metals* **9**, 374–380.

Goodman, S. R., Brenner, S. S. & Low, J. R. 1973 FIM-AP studies of copper precipitation. *Metall. Trans.* **4**, 2363–2377.

PHILOSOPHICAL TRANSACTIONS OF THE ROYAL SOCIETY A MATHEMATICAL, PHYSICAL & ENGINEERING SCIENCES

Greenwood, G. W. 1968 Particle coarsening. In *Proceedings of International Symposium on Mechanism of Phase Transformations in Cystalline Solids*, pp. 103–110. London: Institute of Metals.

Ham, F. S. 1958 Theory of diffusion limited precipitation. *J. Phys. Chem. Solids* **6**, 335–351.

Harbottle, J. E. & Fisher, S. B. 1982 Copper sulphide precipitation in mild steel. *Nature, Lond.* **299**, 139–140.

Hornbogen, E. & Glenn, R. C. 1960 Precipitation of copper in iron. *Trans. metall. Soc. A.I.M.E.* **218**, 1064–1070.

Hornbogen, E. & Jung, H-P. 1964 The nucleation diagram of iron–copper alloys. *Z. Metallk.* **55**, 691–698.

Jones, R. B. & Buswell, J. T. 1984 Preliminary results of an investigation of structure of pressure vessel steels by small angle neutron scattering. In *Proceedings of Conference on Dimensional Stability and Mechanical Behaviour of Irradiated Metals and Alloys, Brighton, April* 1983, vol. 2, pp. 105–106. London: BNES.

Knowles, G. & Kelly, P. M. 1971 Elastic modulus hardening. In *Proceedings of Conference on Effect of Precipitates on Mechanical Properties of Steel*, pp. 9–15. London: Iron and Steel Institute.

Krishnadev, M. R. & Le May, I. 1970 Properties of a copper-bearing steel. *J. Iron Steel Inst.* **208**, 458–462.

Little, E. A. & Harries, D. R. 1970 Effects of nitrogen on radiation hardening. *Metal. Sci. J.* **4**, 188–194.

Lott, R. G., Brenner, S. S., Miller, M. K. & Wolfenden, A. 1981 Development of radiation damage in steels. *Trans. Am. nucl. Soc.* **38**, 303–304.

Odette, G. R. 1979 Neutron exposure dependence of pressure vessel embrittlement. In *Proceedings of IAEA Technical Committee Meeting on Correlation Accuracy in Pressure Vessel Steel*, (ed. W. Schneider), pp. 310–333. Jülich: KFA.

Odette, G. R. & Lombrozo, P. 1983 Physically based model for irradiation embrittlement. *Trans. Am. nucl. Soc.* **44**, 224–225.

Potapovs, U. & Hawthorne, J. R. 1969 Effects of residual elements on response of pressure vessel steels. *Nucl. Appl.* **6**, 27–46.

Russell, K. C. & Brown, L. M. 1972 Dispersion strengthening in iron–copper system. *Acta metall.* **20**, pp. 969–974.

Salje, G. & Feller-Kniepmeier, M. 1977 Diffusion and solubility of copper in iron. *J. appl. Phys.* **48**, 1833–1839.

Tokaku, H. & Tokiwai, M. 1979 The improvement of irradiation–enhanced copper embrittlement. *J. nucl. Mater.* **80**, 57–68.

Wriedt, H. A. & Darken, L. S. 1960 Solubility of copper in ferrite. *Trans. metall. Soc. A.I.M.E.* **218**, 30–34.

PHILOSOPHICAL TRANSACTIONS OF THE ROYAL SOCIETY A MATHEMATICAL, PHYSICAL & ENGINEERING SCIENCES

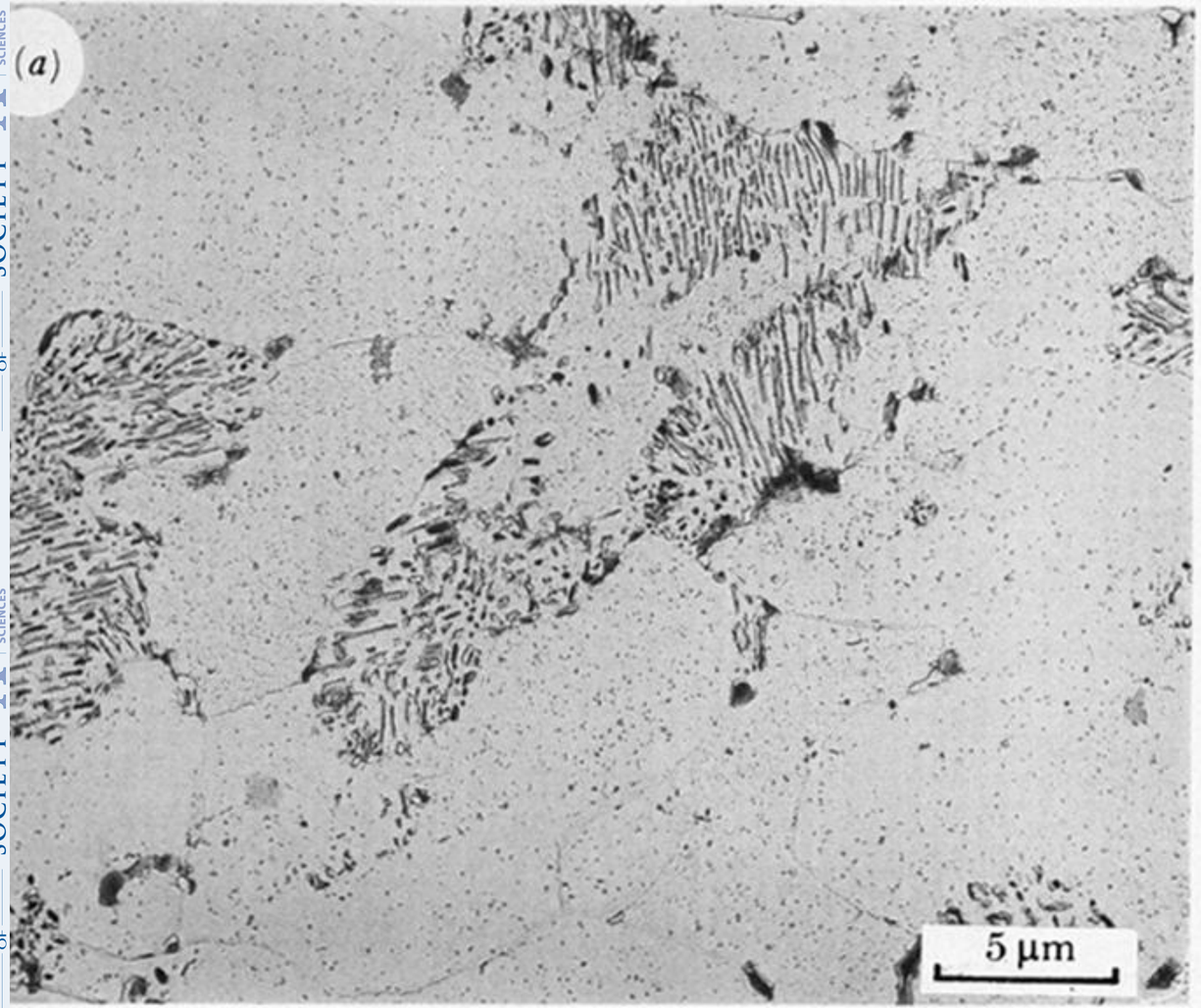

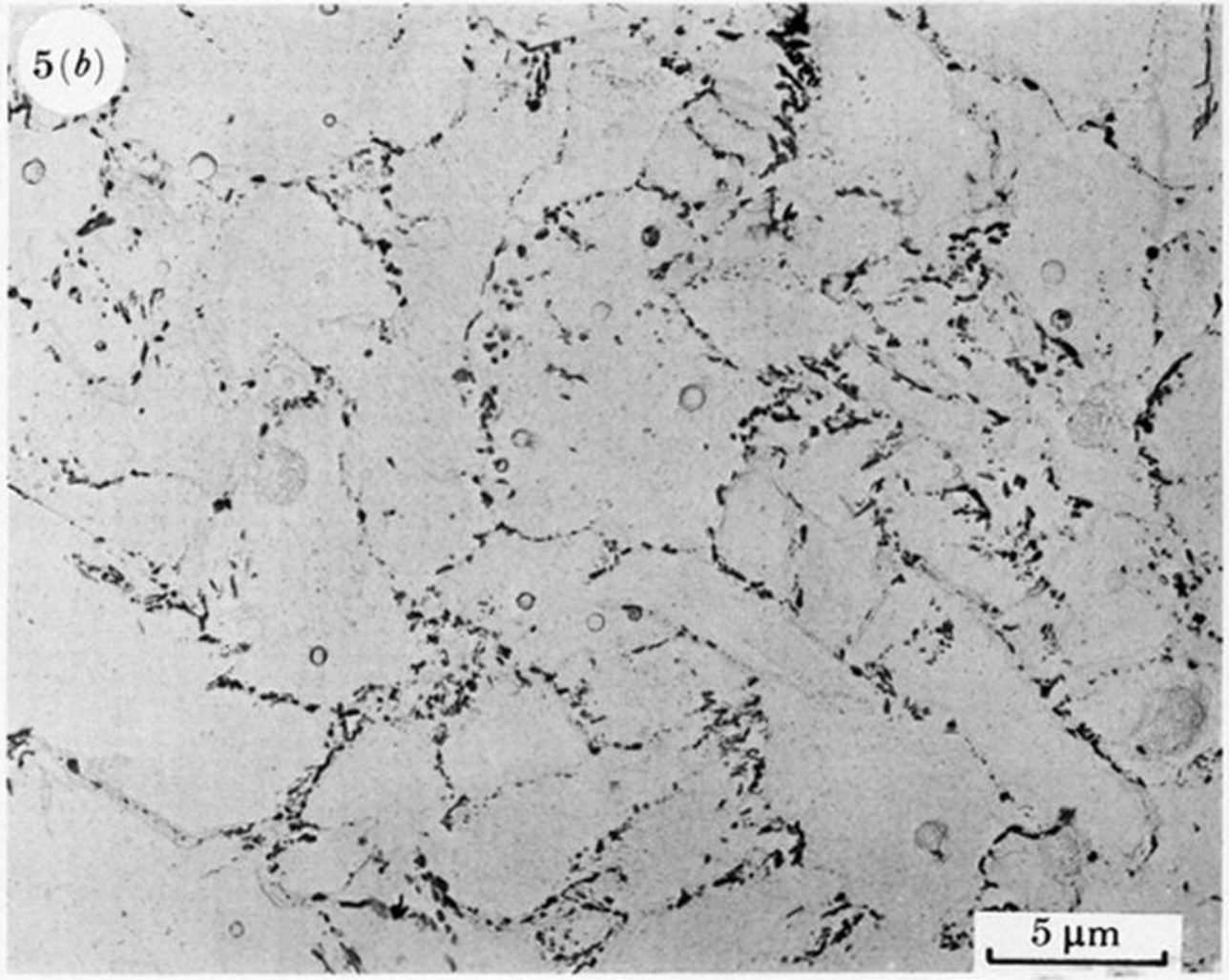

FIGURE 5. The general macrostructures of (*a*) plate and (*b*) weld steels as revealed by carbon extraction replicas.

PHILOSOPHICAL TRANSACTIONS OF THE ROYAL SOCIETY A MATHEMATICAL, PHYSICAL & ENGINEERING SCIENCES

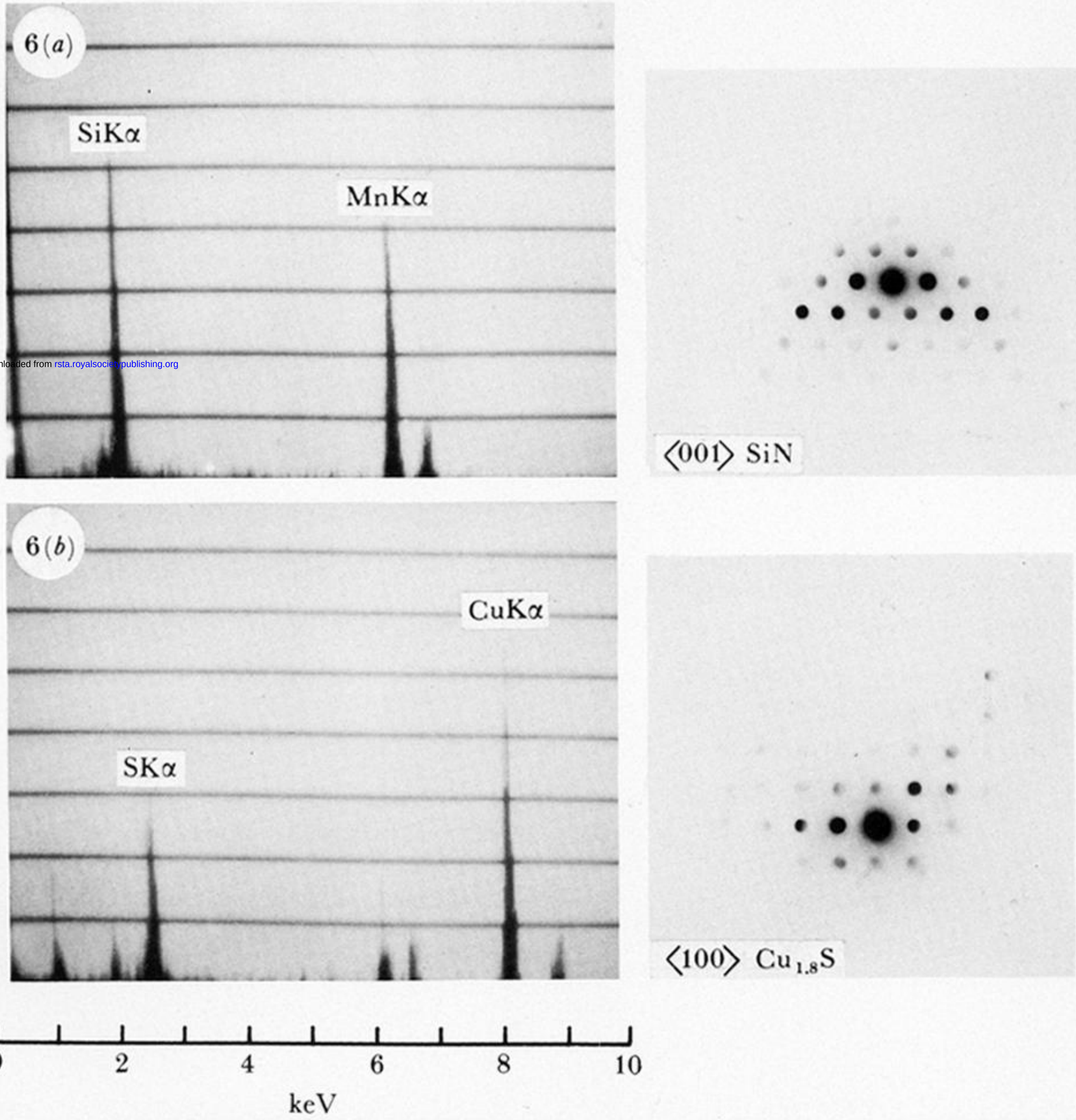

FIGURE 6. The identification of (*a*) (silicon, manganese) nitride and (*b*) copper sulphide precipitates by using a combination of electron diffraction and X-ray energy analysis techniques.

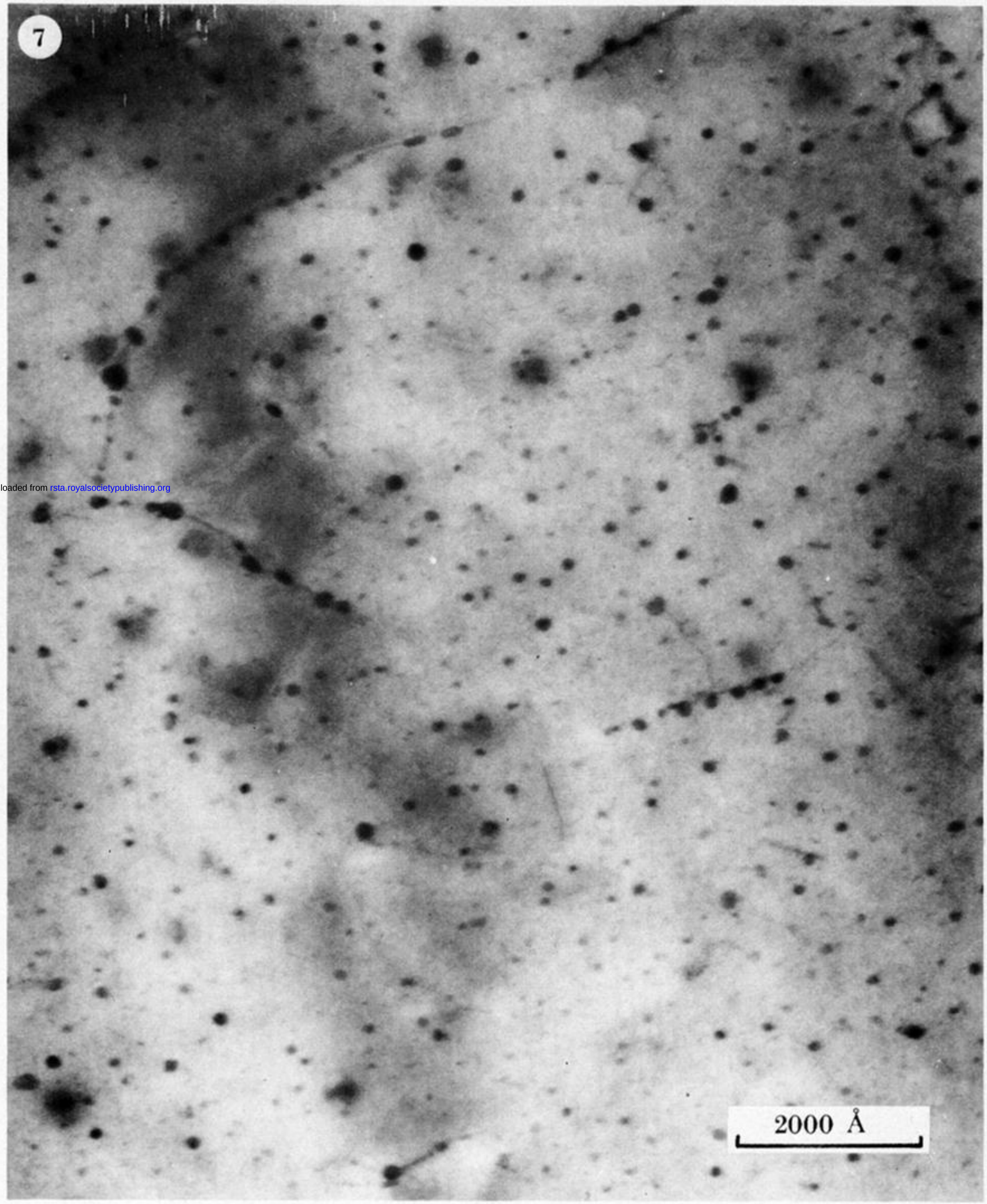

FIGURE 7. Spherical copper precipitates identified in a thin foil of steel I examined in an EM400. The particles are present on both dislocations and within the matrix of this steel after ageing at *ca.* 350 °C for 19600 h. The average precipitate diameter is *ca.* 140 Å, and the volume fraction precipitated is *ca.* 0.35 %.

PHILOSOPHICAL TRANSACTIONS OF THE ROYAL SOCIETY A MATHEMATICAL, PHYSICAL & ENGINEERING SCIENCES